American Mineralogist, Volume 65, pages 690-710, 1980

Relations between the anionic structure and viscosity of silicate melts—a Raman spectroscopic study

BJØRN O. MYSEN, DAVID VIRGO AND CHRISTOPHER M. SCARFE[1]

Geophysical Laboratory, Carnegie Institution of Washington
Washington, D. C. 20008

Abstract

Raman spectroscopy of quenched silicate melts has been used to determine their anionic structure as a function of bulk composition and pressure. The structural results have been integrated with published data on physical and chemical properties of the melts.

The structure of silicate melts on the joins Na_2O–SiO_2, CaO–SiO_2, CaO–MgO–SiO_2, and probably other analogous binary joins, can be described in terms of anionic structural units that, on the average, have NBO/Si = 4, 3, 2, 1, and 0 (NBO/Si: nonbridging oxygens per silicon). Distinct compositional regions involving only three of these structural units have been delineated. These compositional ranges (0–~20, ~20–50, and >50 mole % metal oxide) coincide with compositional ranges defined by thermal expansivity data and data on the activation energy of viscous flow.

Melts on the join $NaAlO_2$–SiO_2 have a three-dimensional array of SiO_4 and AlO_4 tetrahedra. Two three-dimensional units, which differ in Si/(Si + Al), coexist. Both structural units become more aluminous as the bulk Si/(Si + Al) of the system decreases. The structure of these melts remains essentially unaffected as the pressure is increased to 38 kbar. At 1 atm, the viscosity of melts on this join decreases with increasing $NaAlO_2/SiO_2$. This decrease is related to the increased proportion of weaker Al–O relative to Si–O bonds in the three-dimensional structure. The decrease of the melt viscosity with increasing pressure is related to an increase in the number of nearest oxygen neighbors around the metal cations. We suggest that each Al–O bond in the structure is weakened as the result of this process, which results in the lowering of the melt viscosity.

The Raman spectra of melts in the system Na_2O–Al_2O_3–SiO_2 with Al/Na > 1 indicate that nonbridging oxygens are present in the melts. Some aluminum is, therefore, no longer in tetrahedral coordination in the melt. This structural change is responsible for the observed decrease in viscosity and activation energy of viscous flow as Al/Na is increased above 1.

Introduction

Most of the dynamic processes of magma formation and evolution take place in the earth's crust and upper mantle. Most of these processes depend on the viscosity of the magma. It has been shown (*e.g.*, Marsh, 1975; Arndt, 1977) that the percentage of melting necessary for separation of partial melts and residual crystals depends on the melt viscosity. The temperature gradient in a magma chamber required to induce convection also depends on the viscosity of the magma (*e.g.*, Shaw, 1965; Bartlett, 1969). Furthermore, the capacity of a magma to carry material in suspension is directly related to the melt viscosity. Inasmuch as these processes take place at pressures ranging from 1 atm to those corresponding to the upper mantle, it is also necessary to understand the pressure dependence of the viscosity of silicate melts. Such information has recently become available (Kushiro, 1976, 1978a,b,c; Fujii and Kushiro, 1977; Kushiro *et al.*, 1976; Scarfe *et al.*, 1979). Scarfe *et al.* noted that the viscosity of highly polymerized silicate melts decreases with increasing pressure under isothermal conditions. Less polymerized melts (*e.g.*, melts of meta- and disilicate compositions) show a viscosity increase with increasing pressure. Hydrous melts also show an increase in their viscosity with increasing pressure (Shaw, 1963; Kushiro, 1978c).

The viscous behavior of simple binary and ternary

[1] On leave from the University of Alberta, Edmonton, Canada.

0003–004X/80/0708–0690$02.00

melts in systems such as $CaO–Al_2O_3–SiO_2$, $MgO–Al_2O_3–SiO_2$, $Na_2O–Al_2O_3–SiO_2$, and $K_2O–Al_2O_3–SiO_2$ has been used to model the anionic structure of silicate melts (*e.g.,* Bockris *et al.,* 1955; MacKenzie, 1960; Riebling, 1964, 1966; Bockris and Reddy, 1970).

In simple binary metal oxide–silicate systems, the viscosity (η) and activation energy ($E\eta$) of viscous flow of the melts have been used to model their structure. In these models ("discrete polyion model," see Bockris and Reddy, 1970, p. 614 for summary), three distinct compositional ranges (molar metal oxide-silica ratio <20, 20–50, and >50) have been defined within which specific anionic structural units coexist. This model has subsequently been refined with the aid of thermal expansivity and partial molar volume data (see Robinson, 1969, for review of data).

Rheological data have also been used to conclude that melts on joins such as $NaAlO_2–SiO_2$, $CaAl_2O_4–SiO_2$, and $MgAl_2O_4–SiO_2$ have a three-dimensional network structure (Riebling, 1964, 1966). Subsequent RDF (RDF: radial distribution function) data by Taylor and Brown (1979) have confirmed this conclusion. Rheological data in the system $Na_2O–Al_2O_3–SiO_2$ have also been used to infer that nonbridging oxygens exist in melts where Na/Al is different from 1 (Riebling, 1966).

Rather than relying on properties of melts to infer their structure, the structure may be determined directly. A model thus generated can be integrated with data on physical and chemical properties. In an attempt to reach this goal, the anionic structures of a broad range of silicate melts have been determined with Raman spectroscopy at both 1 atm and high pressure.

In this paper, the structural interpretation of the Raman data is presented first. These data are compared with the structural models of silicate melts derived with other techniques. The structural model is then integrated with data on physical and chemical properties (mainly rheological data) and finally applied to more complex magma compositions.

Starting compositions

On the basis of the physical properties of silicate melts, a study of their anionic structure can conveniently be divided into three compositional groups. These are binary metal oxide–silicate melts, aluminosilicate melts with Al^{3+} charge-balanced with metal cations, and aluminosilicate melts where Al^{3+} is not charge-balanced. The compositions are shown in Table 1. The first group includes binary melts on the joins $CaO–SiO_2$, $MgO–CaO–SiO_2$ (Ca/Mg = 1), $Na_2O–SiO_2$, and $Al_2O_3–SiO_2$. With the possible exception of $Al_2O_3–SiO_2$, published spectroscopic data (*e.g.,* Brawer and White, 1975, 1977; Verweij, 1979a,b; Furukawa and White, 1980; Virgo *et al.,* 1980) indicate that in such melts, the ratio of nonbridging oxygen to silicon (NBO/Si) is a simple function of the ratio of metal cations to silicon (M/Si). The system $Al_2O_3–SiO_2$ was chosen to determine whether Al^{3+} is a network former or a network modifier in the absence of local charge-balance of the tetrahedral cation with a mono- or divalent metal. Day and Rindone (1962a,b) suggested on the basis of X-ray data that aluminum is a network modifier whenever the molar metal oxide–aluminum oxide ratio is less than 1. On the other hand, Lacy (1963) has suggested that Al^{3+} probably is not in AlO_6 octahedra because such an arrangement is energetically unfavorable. Lacy therefore suggested the AlO_6-tricluster concept with Al^{3+} in tetrahedral coordination. Melts along a join from Al_2O_3 (10 wt %) SiO_2 (90 wt%) to Al_2O_3 (10 wt%), Na_2O (6 wt%), SiO_2 (84 wt%) were therefore studied, in order to relate the Na/Al of the melt to the structural role of Al^{3+} of the melt.

Table 1. Composition of starting materials (mole %)

	NS2	NS3	NS5	NS9	NS20		
System $Na_2O–SiO_2$							
SiO_2	66.7	75.0	80.0	90.0	95.0		
Na_2O	33.3	25.0	20.0	10.0	5.0		
	WL50	WL25	Wo	SW70	SW40	$CaSi_2O_5$	
System $CaO–SiO_2$							
SiO_2	41.7	45.8	50.0	55.0	60.0	66.7	
CaO	58.3	54.2	50.0	45.0	40.0	33.3	
	DM95	DM85	DM58	DM40	Di	SD70	SD40
System $CaO–MgO–SiO_2$ (Ca/Mg = 1)							
SiO_2	34.2	35.8	40.4	43.4	50.0	55.0	60.0
MgO	32.9	32.1	29.8	28.3	25.0	22.5	20.0
CaO	32.9	32.1	29.8	28.3	25.0	22.5	20.0
	Ne	Jd	Ab	AS 50	$NaAlSi_7O_{16}$	SAN 3	SA 10
System $Na_2O–Al_2O_3–SiO_2$							
SiO_2	50.0	66.6	75.0	80.0	87.5	90.8	93.9
Al_2O_3	25.0	16.7	12.5	10.0	6.3	6.2	6.1
Na_2O	25.0	16.7	12.5	10.0	6.3	3.0	--

The third group of melts was on the join $NaAlO_2–SiO_2$. The viscosity of melts on this join decreases rapidly as a function of decreasing Si/(Si + Al) (Riebling, 1966), despite observations that melts along this join all seem to have a three-dimensional network structure (*e.g.,* Taylor and Brown, 1979; Navrotsky *et al.,* 1980). The viscosity of melts on this join decreases with increasing pressure (Kushiro, 1976, 1978a). This observation has led to suggestions

that Al^{3+} may undergo coordination changes with increasing pressure (Kushiro, 1978a), although Sharma *et al.* (1979) indicated that Al^{3+} remains in tetrahedral coordination even at high pressure. Scarfe *et al.* (1979) also noted that melts on this join are significantly more compressible than Al-free melts with a significant number of nonbridging cations. Selected compositions on this join were therefore subjected to pressures up to 38 kbar.

Experimental technique

The starting materials were prepared from spectroscopically pure (Johnson and Matthey) SiO_2, Al_2O_3, MgO, and $CaCO_3$, and reagent grade Na_2CO_3. These oxides (in batches of less than 200 mg) were ground under alcohol for more than 1 hour and dried at about 400°C. All quenched melts were stored at 110°C prior to acquisition of the Raman data. The quenched melts were made at selected temperatures and pressures within the ranges where viscosities and densities had been determined. One-atm samples were made by quenching the melts in liquid nitrogen in a vertical quench furnace. The quenching rate was approximately 500°C/sec over the first 500–1000°C cooling. High-pressure samples were prepared in a solid-media, high-pressure apparatus (Boyd and England, 1960) with furnace assemblies of 0.5″ diameter. The piston-out technique with 4 percent friction correction (calibrated against the quartz–coesite transition) was used. The temperatures were monitored with Pt–Pt90Rh10 thermocouples. The uncertainty of the temperature is 6–10°C, depending on the temperature of the experiment (Mao *et al.*, 1971). The uncertainty of the pressure is ±1 kbar (Eggler, 1977). The quenching rate in the solid-media, high-pressure apparatus was approximately 250°C/sec over the first 1000°C.

All samples (10–30 mg) both at 1 atm and at high pressure, were prepared in sealed Pt capsules. In the one-atm experiments, alkali metals tend to volatilize (Kracek, 1930; Robinson, 1969; Seifert *et al.*, 1979a) when exposed to air or gases such as CO_2 and CO. This problem is circumvented by sealing the capsules. High-pressure samples were sealed in Pt capsules in order to avoid access of water and other contaminants from the furnace assembly to the sample.

The Raman spectra were taken on small chips of quenched melt (about 0.5–1.0-mm cubes) that were free of bubbles. The spectra were recorded with a Jobin–Yvon optical system, holographic grating, double monochromator (HG25) and a photon-counting detection system. The spectra were recorded at 3 cm^{-1}/sec. The samples were excited with the 488.0 nm line of an Ar^+ laser using a laser power of 200–400 mW at the sample with 90° scattering geometry. Polarized spectra were obtained with the focused exciting beam parallel to the horizontal spectrometer slit and with the electric vector of the exciting radiation in a vertical orientation. A sheet of polarizer disk in front of an optical scrambler was used to record separately the parallel and perpendicular components of the scattered radiation.

As a matter of routine, replicate spectra from the same chips, from different chips of the same experimental run product, and from duplicate experiments were also taken.

The Raman spectra are sensitive to variations of sample composition, which may result from inappropriate sample preparation. Seifert *et al.* (1979a) showed, for example, that sodium loss from melts on the join Na_2O–SiO_2 results in changes of the high-frequency envelope as Na loss results in a decrease of NBO/Si of the melt. The spectra do not indicate such effects.

As discussed below, whenever Na/Al differs from 1 for melts on the join Na_2O–Al_2O_3–SiO_2, Raman bands due to nonbridging oxygens will appear. Thus any heterogeneity of Na/Al/Si of the sample due to inappropriate sample preparation will result in the appearance of bands in the Raman spectra due to nonbridging oxygens. Inasmuch as such bands were never observed, we conclude that the quenched melts were homogeneous.

Incomplete melting of the very viscous melts on the join $NaAlO_2$–SiO_2 will result in Raman spectra with sharp bands, provided that the crystallites are larger than 20–50Å (Brawer, 1975). In this respect, the Raman technique is more sensitive than optical, X-ray, or electron microprobe methods. The absence of such sharp bands in any of the spectra indicates that all samples were completely molten.

Melt *vs.* quenched melt (glass)

In the structural study of silicate melts, quenched melts (glass) have been used. Most of the physical properties discussed later were obtained on molten silicates. In order to relate the structural determinations of quenched melts to the structure of molten silicates, it is necessary to document that the structural features under consideration are not significantly affected by quenching. Riebling (1968) and Taylor *et al.* (1980) found that the anionic units (silicate polymers) in melts with three-dimensional network structure, such as melt of $NaAlSi_3O_8$ composition, remain

the same as the melt is quenched to a glass. Direct experimental proof of structural similarity between melts and glasses on the join Na_2O–SiO_2 was provided by Sweet and White (1969) and Sharma *et al.* (1978). In those studies, infrared and Raman spectra of melts of Na_2SiO_3, $Na_2Si_2O_5$, and $Na_2Si_3O_7$ composition were comparable to the spectra of quenched melts. It was concluded, therefore, that the anionic structural units in these melts are the same before and after quenching.

On the basis of the information given above, we conclude that the structural features of silicate melts

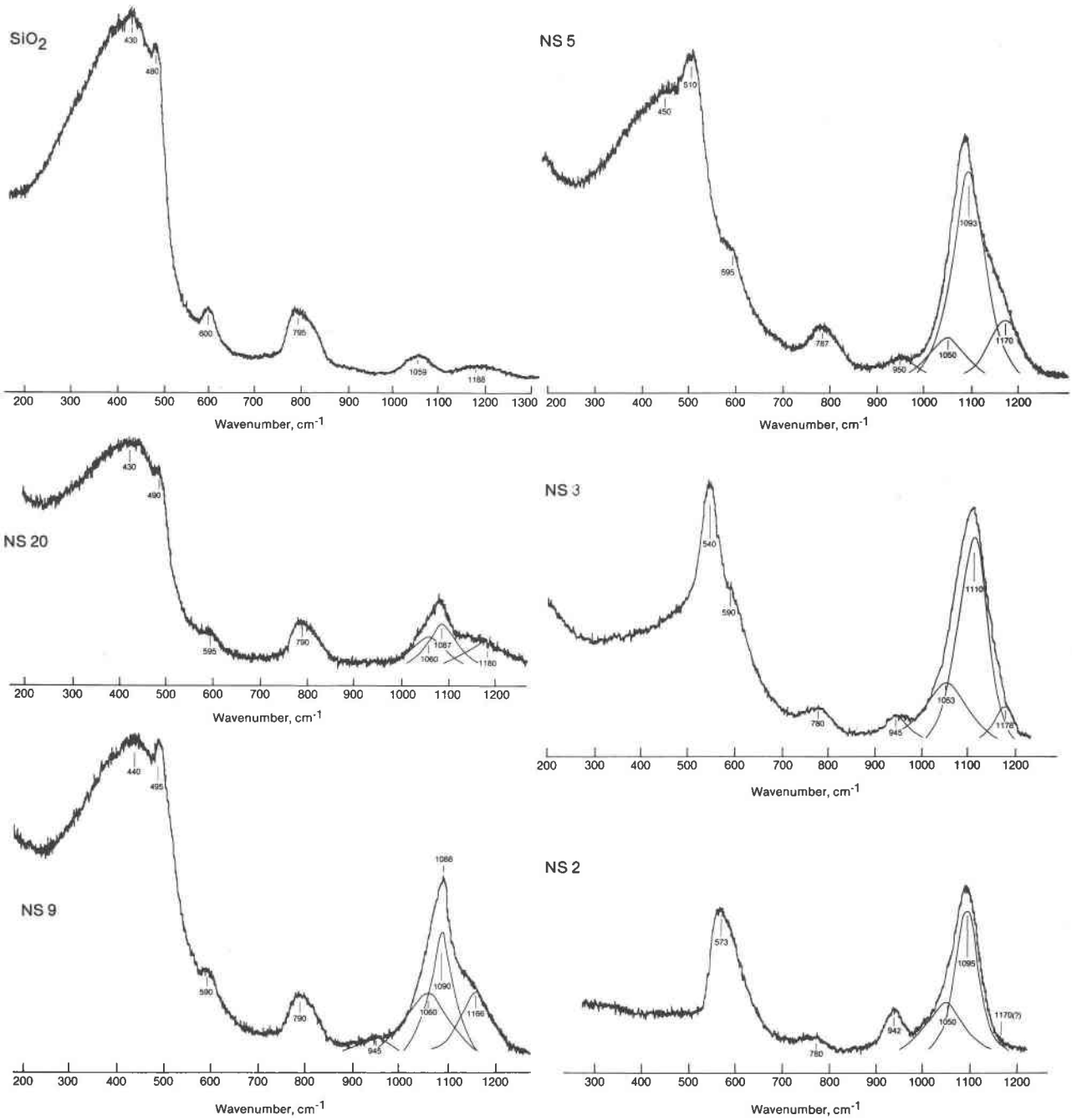

Fig. 1. Raman spectra of quenched melts on the join Na_2O–SiO_2 at 1 atm. See Table 1 for explanation of symbols.

discernible with Raman spectroscopic techniques are quenchable, and the results given in this report are applicable therefore to molten silicates.

Experimental results

1-atm results

Binary joins. The most comprehensive set of structural data on silicate melts is from melts on binary

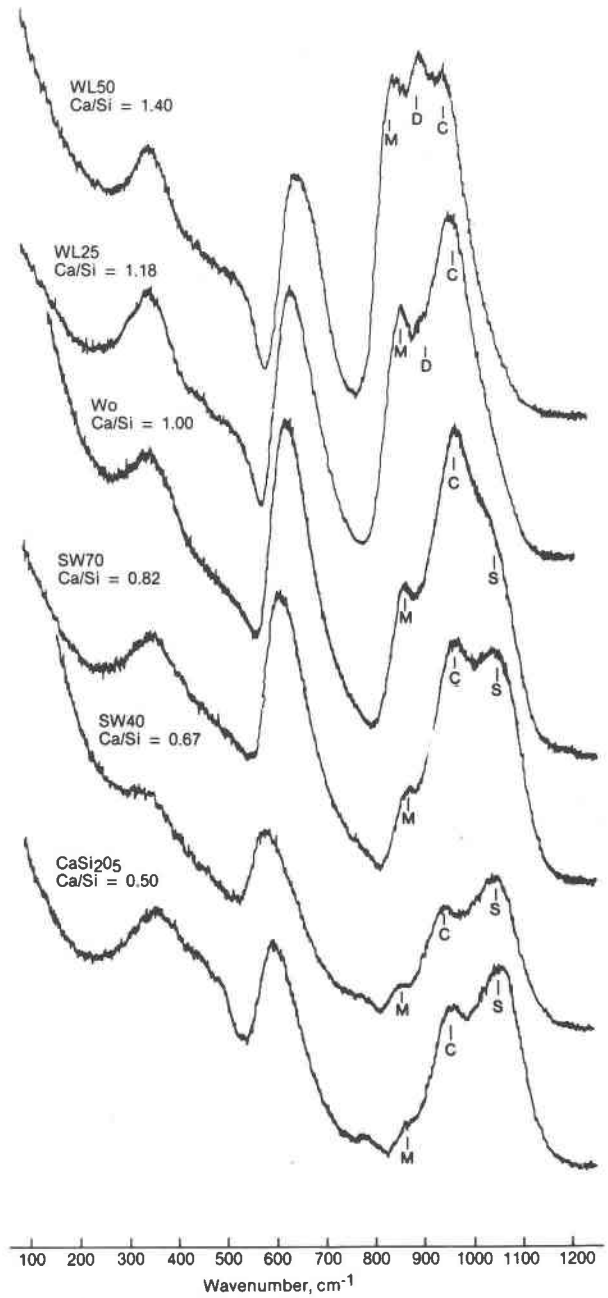

Fig. 2. Raman spectra of quenched melts on the join CaO–SiO_2 at 1 atm. See Table 1 for explanation of symbols. M, D, C, and S refer to monomer, dimer, chain, and sheet species, respectively.

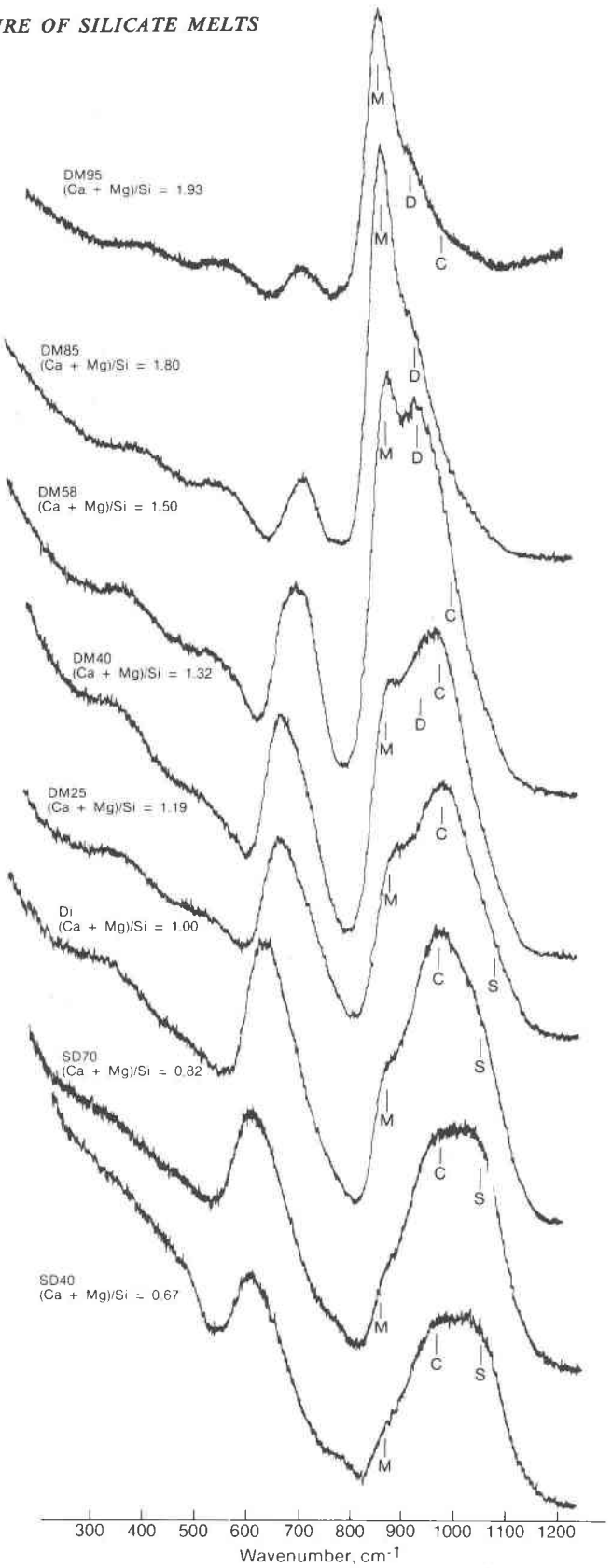

Fig. 3. Raman spectra of quenched melts on the join CaO–MgO–SiO_2 (Ca/Mg = 1) at 1 atm. See Table 1 for explanation of symbols. See Fig. 2 caption.

Table 2. Raman data of quenched melts on metal oxide–silicate joins

Comp.	T, °C	P, kbar	Wavenumber, cm^{-1}											
DM 95	1650	0.001	380w,p,(bd)	–	530m,p,(bd)	700w,p	–	848s,p	903m,p	977mw,p	***	–	–	
DM 85	1650	0.001	380w,p,(bd)	–	527m,p,(bd)	700w,p	–	847s,p	903m,p	978m,p	***	–	–	
DM 58	1650	0.001	343w,p,(bd)	–	513m,p,(bd)	686m,p	–	860s,p	910s,p	973m,p	***	–	–	
DM 40	1650	0.001	340w,p,(bd)	–	500m,p,(bd)	660m,p	–	863s,p	908mw,p	973m,p	***	–	–	
DM 25	1650	0.001	340w,p,(bd)	–	–	655m,p	–	860s,p	913w,p	973s,p	***	–	–	
Di	1650	0.001	340w,p,(bd)	–	–	630m,p	770vw,(sh)	867m,p	–	967s,p	***	1060m,p	–	
SD 70	1650	0.001	–	–	–	622s,p	770w	873w,p	–	959s,p	***	1063m,p	–	
SD 40	1650	0.001	–	–	500vw,(sh)	610s,p	–	873vw	–	955s,p	***	1063m,p	–	
WL 50	1650	0.001	352m,p	–	547w,(sh)	670s,p	–	850s,p	900s,p	960s,p	***	–	–	
WL 25	1650	0.001	350m,p	–	547w,(sh)	647s,p	–	851s,p	907s,p	980s,p	1059w	–	–	
Wo	1650	0.001	345m,p,(bd)	–	–	620s,p	–	867s,p	–	962s,p	***	1050m,p	–	
SW 70	1650	0.001	–	–	–	613s,p	–	869w,p	–	963s,p	***	1051s,p	–	
SW 40	1650	0.001	–	–	–	586s,p	–	863vw	–	957s,p	***	1055s,p	–	
$CaSi_2O_5$	1650	0.001	–	–	–	593s,p	–	861vw	–	958s,p	***	1057s,p	–	
NS 2	1500	0.001	–	–	–	573s,p	780vw	–	–	942m,p	1050m	1095s,p	–	
NS 3	1500	0.001	–	–	480w,(sh)	540s,p	780w	–	–	945w,p	1053m	1105s,p	1170vw(?)	
NS 5	1500	0.001	–	450m,p	490s,p	–	787m	–	–	950w,p	1050m	1093s,p	1178m	
NS 9	1650	0.001	–	440s,p	495s,p	–	790m	–	–	945vw	1060m	1087s,p	1166m	
NS 20	1650	0.001	–	430s,p	490s,p	–	790m	–	–	–	1060m	1090s,p	1180m	
NS 2	1200	0.001	–	–	–	564s,p	760w	–	–	940m,p	1050m	1095s,p	***(?)	
NS 2	1200	15	–	–	–	564s,p	758w	–	–	937m,p	1060m	1095s,p	***(?)	
NS 2	1200	25	–	–	–	573s,p	763w	–	–	948m,p	1060m	1103s,p	***(?)	
Di	1425	0.001	–	–	–	633s,p	–	880m,p	–	980s,p	***	1068(sh)	–	
Di	1550	0.001	–	–	–	632s,p	–	880m,p	–	983s,p	***	1070(sh)	–	
Di	1650	10	–	–	–	629s,p	–	873(sh)	–	975s,p	***	1070(sh)	–	
Di	1650	20	–	–	–	629s,p	–	873(sh)	–	975s,p	***	1070(sh)	–	
Di	1685	20	–	–	–	636s,p	–	873(sh)	–	978s,p	***	1066(sh)	–	
NS 3	1300	0.001	–	–	538s,p	–	773w	–		950w,p	1050m	1107s,p	***	
NS 3	1300	15	–	–	544s,p	–	773w	–	–	950w,p	1070m	1105s,p	***	

Abbreviations: vw, very weak; w, weak; mw, medium to weak; m, medium; ms, medium to strong; s, strong; p, polarized; (bd), broad; (sh), shoulder. Compositional notations are defined in Table 1.

Uncertainties: Strong to weak bands, ± ~5 cm^{-1}. Very weak bands, ~10 cm^{-1}. Shoulders, 15–20 cm^{-1}.

metal oxide–silicate joins. It is convenient, therefore, to discuss these data first (Figs. 1–3; Table 2). Raman and infrared data on such joins have been published by Brawer and White (1975, 1977), Sweet and White (1969), Furukawa *et al.* (1978), Furukawa and White (1980), Verweij and Konijnendijk (1976) and Verweij (1979a,b). A summary of these data was provided by Virgo *et al.* (1980).

In the present study, the joins Na_2O–SiO_2, CaO–SiO_2, and CaO–MgO–SiO_2 have been emphasized. Inasmuch as the alkaline earth–silicate joins are intersected by a liquid immiscibility gap near $M^{2+}/(Si^{4+}+M^{2+}) = 0.3$, our studies were limited to melts with a larger $M^{2+}/(Si^{4+}+M^{2+})$. The Na_2O–SiO_2 join was extended to pure SiO_2, as there is no stable liquid immiscibility on this join.

(a) Na_2O-SiO_2: The Raman spectra of six quenched melts on the join Na_2O–SiO_2 are shown in Figure 1 (see also Table 2). The high-frequency envelope between 800 and 1200 cm^{-1} was deconvoluted into individual bands with Gaussian line-shape by the following technique. First it was assumed that the background in this spectroscopic range was horizontal. This assumption is an approximation, as the Rayleigh tail has an exponential form. Extrapolation of the Rayleigh tail from less than 500 cm^{-1} to the region of interest with exponential equations indicates less than 5% deviation from a horizontal background at wavenumbers greater than about 800 cm^{-1}. Second, all bands were considered symmetric. Third, bands were fitted to the high-frequency envelope only when their existence was indicated by separate peaks or shoulders or abrupt deviations from Gaussian line shape of portions of the high-frequency envelope.

With these considerations in mind, the spectra of quenched melts on the join Na_2O–SiO_2 will be discussed (Fig. 1; see also Table 2). The Raman spectrum of one of the endmembers, SiO_2, has been discussed in detail elsewhere (*e.g.*, Bell and Dean, 1970, 1972; Bates *et al.*, 1974; Stolen and Walrafen, 1976; Galeener and Lucovsky, 1976a,b; Lucovsky, 1979a,b). The Raman spectrum consists of a strong, broad band near 430 cm^{-1} and a less intense, sharp band near 480 cm^{-1} (Fig. 1). There are weak bands at 600, 795, 1059, and 1188 cm^{-1}. All but the 795, 1059, and 1188 bands are polarized. The 430 and 795 cm^{-1} bands represent oxygen bending motions with some contribution from the silicon atom in the 795 cm^{-1} (Lucovsky, 1979a). The 480 cm^{-1} band is a rocking band that stems from rocking of bridging oxygen bonds in a fully polymerized, three-dimensional network (Bates *et al.*, 1974; Bell and Dean, 1972). The band near 600 cm^{-1} most likely is due to bending motions of oxygen bonds in defect structures in quenched SiO_2 melt (Lucovsky, 1979a,b). This defect is generated by breaking one Si–O bridging bond in the continous three-dimensional network. The defect

density in quenched, anhydrous SiO_2 melt is approximately 10^{19} cm^{-3} (Stolen and Walrafen, 1976; Lucovsky, 1979a), which implies that about 0.01% of the ideally bridging oxygen bonds have been broken.

The 1059 and 1188 cm^{-1} bands are due to antisymmetric stretch vibrations in a three-dimensional array of SiO_4 tetrahedra. If this array is homogeneous, only one antisymmetric stretch band would be expected (Bell and Dean, 1972). Galeener and Lucovsky (1976a,b) suggested that the two bands result from LO and TO splitting. Inasmuch as LO and TO splitting require long-range order, this interpretation is unlikely in view of the disordered nature of silicate melts. We suggest instead that the two antisymmetric stretch bands are due to two distinct three-dimensional structural units in the quenched melt. The need to consider models of quenched SiO_2 melt on the basis of more than one type of three-dimensional network has also been suggested from high-resolution electron-microscopic studies (Gaskell, 1975; Gaskell and Mistry, 1979; Bando and Ishizuka, 1979).

With 5 mole% Na_2O added to SiO_2 melt (NS20), a new, sharp band appears near 1100 cm^{-1} (Fig. 1). This band becomes more intense relative to all the other bands in the high-frequency envelope as the Na^+/Si^{4+} of the quenched melts is further increased. Another very weak band appears near 950 cm^{-1} in NS9 melt ($Na^+/Si^{4+} = 0.22$) and grows in intensity with increasing Na^+/Si^{4+}. Brawer and White (1975) and Furukawa and White (1980) extended their studies of melt structure on the join Na_2O–SiO_2 to sodium metasilicate (NS). In the compositional range from NS2 to NS, the intensity of the 950 cm^{-1} continued to increase and is the dominant feature of the spectrum of quenched sodium metasilicate melt. In the same compositional range the intensity of the 1100 cm^{-1} band showed a continuous decrease. Neither the 1100 nor the 950 cm^{-1} band showed significant frequency changes in the compositional range between NS20 ($Na^+/Si^{4+} = 0.11$) and NS2 ($Na^+/Si^{4+} = 1$) in the present study and between $Na^+/Si^{4+} = 0.2$ and 2 in the study by Brawer and White (1975). Both the 950 and 1100 cm^{-1} bands also remain polarized in the entire compositional range.

The band near 490 cm^{-1} in the spectrum of quenched NS20 melt becomes more intense and shifts toward 570 cm^{-1} with increasing Na/Si. In quenched NS2 melt ($Na^+/Si^{4+} = 1.0$) the band is at 570 cm^{-1}, where it is the second most intense band in the spectrum. The 490–570 cm^{-1} band remains polarized in the entire compositional range.

The 1100 and the associated 570 cm^{-1} bands are the two strongest bands in crystalline $Na_2Si_2O_5$ whether the α or the β forms are considered (Furukawa and White, 1980). The 950 cm^{-1} band is the strongest band in crystalline metasilicates (Etchepare, 1972; Brawer and White, 1975). Furukawa and White (1980) also noted that the 1100 cm^{-1} band is strongly polarized. The band is IR inactive (White *et al.*, 1979). On the basis of such considerations, Furukawa and White (1980) concluded that the 1100 cm^{-1} band is due to symmetric ^-O–Si–O^0 stretching. Verweij (1979a,b) arrived at a similar conclusion. The 570 cm^{-1} band is due to symmetric stretching of bridging oxygen bonds within the same structural unit as that giving rise to the 1100 cm^{-1} band. The 1050 cm^{-1} band is due to antisymmetric stretching of bridging oxygen bonds in any structure where oxygen bridges exist. The 950 cm^{-1} band is assigned to symmetric ^-O–Si–O^- stretching.

The ^-O–Si–O^- stretch vibrations may be derived from a chain or a ring structure (NBO/Si = 2) and

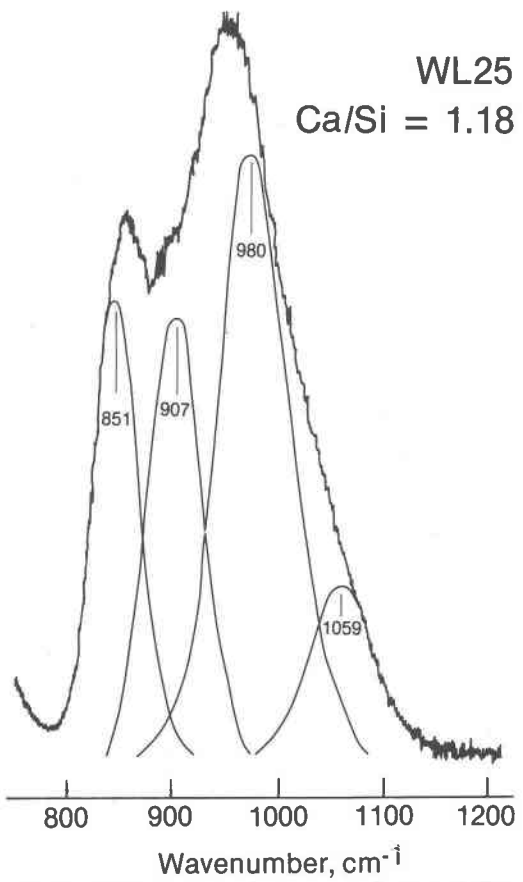

Fig. 4. Quenched WL25 melt deconvolution using Gaussian curves. See text for detailed explanation of procedures.

Table 3. Raman frequencies of the stretch vibrations of specific Si-rich anionic structural units in silicate melts

Structural unit	NBO/Si	Frequency (cm^{-1})	Characteristics of vibrational mode
SiO_4^{4-}	4	850-880	symmetric stretch
$Si_2O_7^{6-}$	3	900-920	symmetric stretch
$Si_2O_6^{4-}$	2	950-980	symmetric stretch
$Si_2O_5^{2-}$	1	1050-1100	symmetric stretch
SiO_2	0	1060,1190	antisymmetric stretch

the $^-O–Si–O^0$ vibration from a structural unit that has NBO/Si ~ 1 (*e.g.*, sheet). Further discussion of these specific structural assignments will be provided after discussion of the spectra of quenched melts on the joins $CaO–SiO_2$ and $CaO–MgO–SiO_2$.

The Raman bands characteristic of three-dimensional network structural units in the melt (430, 800, and 1188 cm^{-1} bands) diminish in intensity in the compositional range between SiO_2 and NS3. The 430, 800, and 1188 cm^{-1} bands are definitely present in the spectra of melts with as much as 25 mole% Na_2O (Na^+/Si^{4+} = 0.67). In the sodium disilicate quenched melt (33 mole% Na_2O), the band near 800 cm^{-1} remains. There is no clear band at frequencies below about 570 cm^{-1}. The Rayleigh tail flattens out between 400 and 500 cm^{-1}, however, which indicates a weak band in this spectral region. We conclude, therefore, that three-dimensional network structural units (3D) definitely exist in melts in the compositional range between SiO_2 and Na^+/Si^{4+} = 0.67 (NS3 melt). This compositional region may extend as far as Na^+/Si^{4+} = 1.0 (NS2 melt).

(b) $CaO–SiO_2$ and $MgO–CaO–SiO_2$ (Ca/Mg = 1): The Raman spectra of quenched melts on the joins $CaO–SiO_2$ and $MgO–CaO–SiO_2$ are shown in Figures 2 and 3 (see also Table 2). The dominant feature of each spectrum is the intense, slightly asymmetric band in the region between about 600 and 670 cm^{-1} combined with an intense, high-frequency envelope in the region between 800 and 1100 cm^{-1}. All these bands are strongly polarized. The Raman spectra of quenched melts on the join $CaO–MgO–SiO_2$ are similar to those on the join $CaO–SiO_2$ (Figs. 2 and 3). The high-frequency envelope of the spectra is somewhat less resolved in the system $MgO–CaO–SiO_2$, however, presumably because of more local disorder in the former system (Brawer, 1975). All the bands, with the exception of that in the 600–670 cm^{-1} region, remain at the same frequency as M^{2+}/Si^{4+} varies (Figs. 2 and 3).

There are at least two bands in these spectra that do not occur in the compositional range of the $Na_2O–SiO_2$ system shown in Figure 1 (compare Fig. 1 with Figs. 2 and 3; see also Table 2). In melts with M/Si between 1.9 (DM 95) and 1.18 (DM 25 and WL 25), there is a very strong sharp band near 870 cm^{-1} and a less intense band near 900 cm^{-1}. Their frequencies are independent of M/Si of the quenched melts (Tables 1 and 2). The 870 cm^{-1} band remains in all spectra of melt compositions from DM 95 to $CaSi_2O_5$ (Ca/Si = 0.5). The 900 cm^{-1} band disappears at melt compositions between DM 25 (M/Si = 1.18) and Di (M/Si = 1). The intensities of both bands decrease as the M/Si decreases. The intensity of the 900 cm^{-1} band probably passes through a maximum relative to the other bands in the high-frequency envelope in melt compositions with M/Si near 1.5 (DM 58 and WL 50; see Table 1). Both bands remain polarized in the entire compositional range.

Table 4. Raman data of quenched melts on the join $Na_2O–Al_2O_3–SiO_2$

Comp.	T °C	P, kbar	Wavenumber, cm^{-1}								
								I_1		I_2	I_2/I_1
Ne	1550	0.001	-	480s,p	561m,p	790w	-	945w,p	-	1014s	3.6
Jd	1450	0.001	-	468s,p	567m,p	767(sh)	-	959m,p	-	1063s	2.2
Ab	1500	0.001	-	470s,p	566w,p	780(sh)	-	983w,p	-	1090s	2.8
AS 50	1650	0.001	440s,p	485(sh)	595w,p	793m	-	987m,p	-	1110s	2.2
$NaAlSi_7O_{16}$	1650	0.001	440s,p	480(sh)	587w,p	793m	-	1023m,p	-	1150m	1.1
SiO_2	1750	0.001	430s,p	483s,p	595w,p	790m	-	1059w	-	1188m	< 1
SA 10	1650	0.001	430s,p	483s,p	600m,p	794m	950w,p	1052m	1117mw,p	1190m	
SAN 3	1650	0.001	431s,p	483(sh)	590m,p	793m	943w,p	1045m	1120w,p	1177m	
Jd	1500	20	-	479s,p	566w,p	782(sh)	-	955m,p	-	1064s	3.5
Jd	1550	38	-	477s,p	561w,p	790(sh)	-	960m,p	-	1060s	5.4
Ab	1500	20	-	468s,p	573w,p	794(sh)	-	980m,p	-	1088s	3.0
Ab	1550	38	-	467s,p	580(sh)	795(sh)	-	970m,p	-	1080s	5.0

Abbreviations and uncertainties: see Table 2.

The 870 cm^{-1} band is by far the most intense band in crystalline orthosilicates (Furukawa *et al.*, 1978; Verweij and Konijnendijk, 1976). Furukawa *et al.* (1978), Verweij and Konijnendijk (1976), and Verweij (1979a,b) assigned this band to symmetric stretch vibrations of nonbridging oxygen bonds in separate SiO_4^{4-} tetrahedral (symbol:$Si-O^{2-}$). This assignment is retained here.

The 900 cm^{-1} band is the major band in crystalline pyrosilicates (Lazarev, 1972; Sharma and Yoder, 1979). In view of the facts that its frequency is higher than that of the symmetric $Si-O^{2-}$ stretch band (870 cm^{-1}), that it is polarized, and that its frequency coincides with the main band in crystalline pyrosilicates, this band is interpreted as due to the presence of dimer structural units ($Si_2O_7^{6-}$) in the melts. Its frequency is independent of NBO/Si of the melt. We conclude, therefore, that the NBO/Si of this structural unit does not change with composition of the melt. Further support for this interpretation is found in the observation that the maximum intensity is found in spectra from melts with NBO/Si near 3 and the fact that it is associated with another band near 700 cm^{-1}. According to Lazarev (1972), the 700 cm^{-1} band in crystalline pyrosilicates is a symmetric stretch vibration of bridging oxygen bonds. Its frequency is characteristic of dimers.

Structural units with NBO/Si ~ 2 occur in all melts discussed so far (Figs. 1–3). Provided that there are structural units with more than three Si^{4+} cations, a Raman band near 1050 cm^{-1} (antisymmetric $Si-O^0$ stretch band) is expected (Furukawa and White, 1980). This band could be discerned in melts on the Na_2O-SiO_2 join with Na^+/Si^{4+} less than about 1 (disilicate). White *et al.* (1979) commented that this band also occurs in melts as depolymerized as metasilicates. It is expected that this band would also be present in quenched melts on the alkaline earth–silicate joins (Figs. 2 and 3). In alkaline earth silicate melts with $M^{2+}/Si^{4+} < 1$, there is also a band due to symmetric $^-O-Si-O^0$ stretching in the immediate vicinity of 1050 cm^{-1}. The high-frequency envelopes of these spectra do not indicate the presence of more than one band, except that it does not seem possible to fit any segment of the high-frequency limb of the envelopes to a single Gaussian equation. In melts

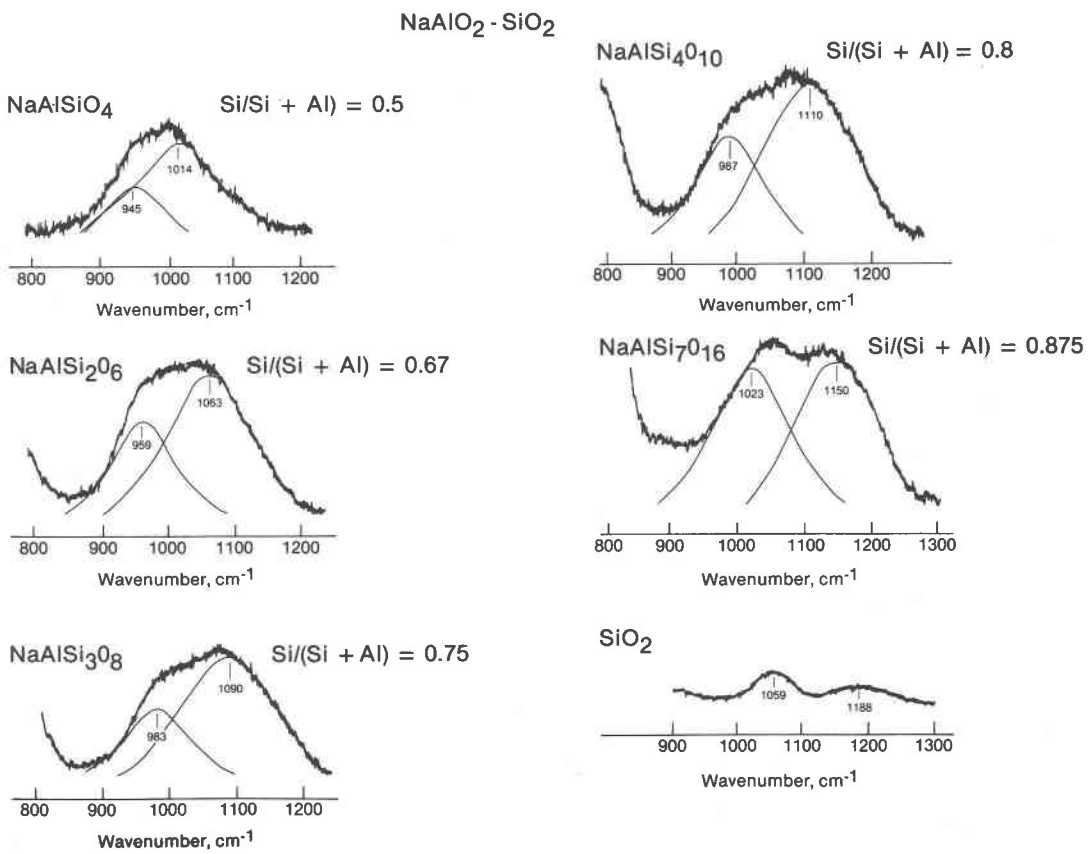

Fig. 5. Raman spectra of quenched melts on the join $NaAlO_2$–SiO_2 at 1 atm. See text for explanation of symbols.

that are less polymerized than metasilicate, only ^{-}O–Si–O^{-}, Si–O^{2-}, and vibrations from dimers occur in the high-frequency envelope. The high-frequency envelope of the spectrum from WL 25 (M/Si = 1.18) indicates that the 970 cm^{-1} is quite broad, however, thus suggesting the presence of a possible fourth band (Figs. 2 and 3). In Figure 4, WL 25 was used in an attempt to fit a band near 1050 cm^{-1} using the technique described above. In Table 2, the presence of this band together with the symmetric ^{-}O–Si–O^{0} stretch band has been only inferred. The reported frequency of this band is, therefore, more uncertain than those of other bands. A summary of band positions and assignments is given in Table 3.

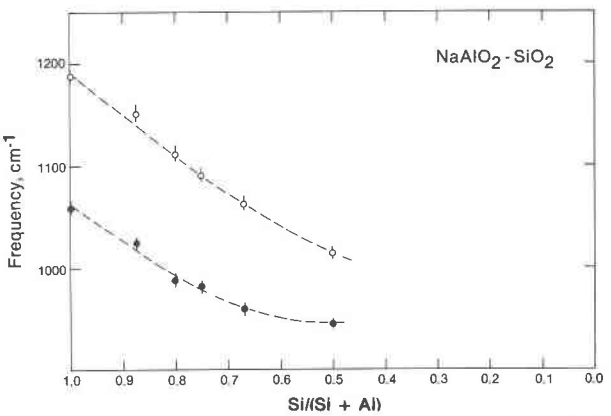

Fig. 6. Frequencies of the two Raman bands in the high-frequency envelope of melts on the join $NaAlO_2$–SiO_2.

Aluminosilicates.

(a) The join $NaAlO_2$–SiO_2: Raman data of quenched melts of six compositions between $NaAlSiO_4$ (Ne) and SiO_2 are given in Table 4. The high-frequency envelopes of the spectra are shown in Figure 5. The Raman data show an overall similarity in the compositional range under consideration. There is a broad, strong, polarized band below 500 cm^{-1}. For melt compositions between $NaAlSi_4O_{10}$ (AS50) and SiO_2, this band is split into one band near 440 cm^{-1} and one between 480 and 490 cm^{-1}. The latter band develops from a shoulder to a separate band with increasing Si/(Si + Al). In addition to these bands, all spectra show weak bands near 600 and 800 cm^{-1}. These bands are polarized. There is, therefore, no principal difference between the spectra of Al-bearing melts and SiO_2 on this join in the range between 400 and 800 cm^{-1}.

The high-frequency envelope (Fig. 5) consists of two bands that occur as distinct peaks in melts with Si/(Si + Al) greater than about 0.8 and as two shoulders with melts that have lower Si/(Si + Al). Their frequencies are lowered as a continuous function of decreasing Si/(Si + Al) (Fig. 6). It also appears that the highest frequency band becomes more intense relative to the lower-frequency band as the Si/(Si + Al) of the melt decreases (Table 4).

The frequencies and the polarization characteristics of all the bands below the high-frequency envelope are nearly identical to those of quenched SiO_2 melt. We suggest, therefore, that these bands are due to the same vibrations in all the melts studied on the join $NaAlO_2$–SiO_2. On this basis, we conclude that the melts on this join consist of an array of three-dimensional SiO_4 and AlO_4 tetrahedra. Taylor and Brown (1979), on the basis of RDF X-ray data, also concluded that sodium aluminum silicates with Na/Al = 1 most likely have a three-dimensional network structure, in agreement with our conclusion.

Virgo *et al.* (1979) studied the frequency shifts of the two high-frequency bands in systems where the T cation was Al^{3+}, Fe^{3+}, or Ga^{3+}. The metal cations were Na^{+} and Ca^{2+}. In all the compositions they studied, the frequencies of the two stretch bands decreased as a function of decreasing Si/(Si + T). Brawer and White (1977) made similar observations in the system CaO–Al_2O_3–SiO_2. Brawer and White (1977) and Virgo *et al.* (1979) suggested that the decrease of the frequency was due to an increased extent of coupling of the Si–O^{0} and T–O^{0} antisymmetric stretch vibrations. Because of the smaller force constants of bonds such as Al–O^{0} compared with Si–O^{0}, the frequency of a coupled band would decrease with increasing Al content of the melt.

The existence of two stretch bands in melts on the join $NaAlO_2$–SiO_2 as well as in the other joins studied by Virgo *et al.* (1979) has been suggested by them to stem from two types of three-dimensional structures in the melts. These structures differ in Si/(Si + T) (Virgo *et al.*, 1979). These authors also noted that of these two bands, the highest-frequency band was more sensitive to compositional changes than the lower-frequency band. They concluded, therefore, that the three-dimensional structure resulting in the highest-frequency band had the largest proportion of T cation. This conclusion is also adopted here. All the quenched melts on the join $NaAlO_2$–SiO_2 have a three-dimensional network structure, therefore, and the tetrahedra become increasingly aluminous with increasing Al content of the melt. The aluminum is, however, partitioned between two apparently distinct tetrahedral units. This conclusion is also in agreement with data from Flood and Knapp (1968). They

calculated liquidus temperatures in the system $NaAlSi_3O_8$–$CaAl_2Si_2O_8$ with the assumption that the structural units in the melts mixed ideally. The agreement between calculated and experimental liquidus data was best when they used two three-dimensional units in the melt. These two structural units differed in Si/(Si + Al).

(b) Melts with Na/Al < 1: It has been suggested (*e.g.*, Day and Rindone, 1962a,b; Riebling, 1964, 1966) that if Al were added to melts on the $NaAlO_2$–SiO_2 join, the extra Al may not be tetrahedrally coordinated, and is, instead, a network modifier.

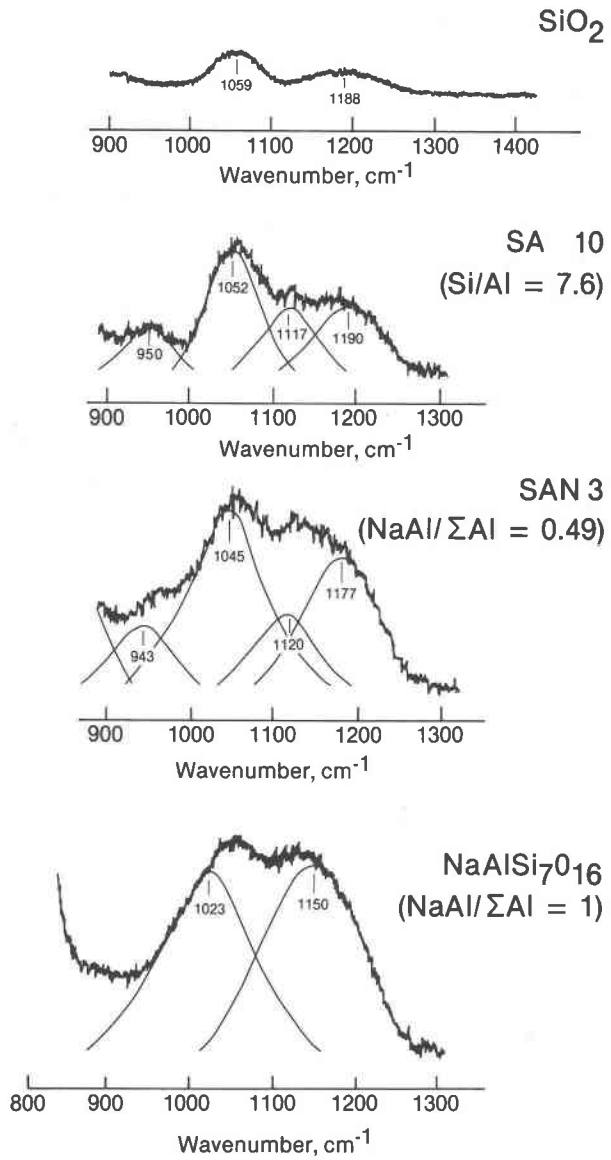

Fig. 7. Raman spectra of quenched melts with Na/Al equal to and less than 1. See Table 1 for explanation of symbols.

Lacy (1963), on the other hand, suggested that AlO_6 octahedra would not be geometrically and energetically stable, and suggested that AlO_6 triclusters were formed instead. No new nonbridging oxygens would be formed in this process. Inasmuch as AlO_6 octahedra occur in minerals, it is not clear why Lacy (1963) concluded that AlO_6 octahedra probably did not occur in silicate melts. To our knowledge, no silicate mineral is known where Al is in tetrahedral coordination without some form of charge balance.

The melt compositions SA10, SAN3 and $NaAlSi_7O_{16}$ were prepared to evaluate the proposed roles of Al^{3+} in silicate melts. These compositions differ in Na/Al ratio (Table 1). The Raman spectra of these melts are shown in Figure 7 (see also Table 4). The portion of the spectra below about 800 cm^{-1} is not significantly different from that of quenched SiO_2 melt. We conclude, therefore, that a large proportion of the melts has a three-dimensional network structure. In SA10 quenched melt there are, however, two additional bands in the high-frequency envelope (near 1100 and near 950 cm^{-1}; see Fig. 7). Both bands are polarized and become less intense as 3 wt% Na_2O (SAN3) is added to SA10. In quenched SA10 melt, the two strongest bands, at 1050 and 1190 cm^{-1}, probably are the two antisymmetric Si–O^0 stretch bands that are also found in quenched SiO_2 melt. The frequencies and polarization characteristics of the two bands near 950 and 1100 cm^{-1} are nearly identical to those found in binary melts on the join Na_2O–SiO_2 (Fig. 1) and could be due to the same vibrations in the melt ($^-$O–Si–O^- and $^-$O–Si–O^0 symmetric stretching).

Provided that the 950 and 1100 cm^{-1} bands are, in fact, due to silicate stretch vibrations in structural units with nonbridging oxygens, it must be concluded that in SA10 quenched melt there is no evidence for Si(Al) coupling, as the frequencies of the four bands in the high-frequency envelope are similar to those in analogous Al-free silicate melts. If this conclusion is correct, the Al in quenched SA10 melt is a network modifier.

Consider now the possibility that the two bands are stretch vibrations involving Al in tetrahedral coordination. With the assumption that both bands are coupled in the same manner as the antisymmetric stretch bands of melts on the join $NaAlO_2$–SiO_2, the data for SA10 are inconsistent with the data in Figure 6. If the band near 1100 cm^{-1} is a coupled stretch vibration, the second band would be near 1000 cm^{-1}, whereas in fact the second band occurs near 950 cm^{-1}. If the 950 cm^{-1} band was an Si(Al)-coupled vi-

bration in a three-dimensional network structure, the associated band would fall near 1000 cm^{-1}, where there is no band. We conclude, therefore, that at least one of the two additional bands is an Si–O stretch band indicative of nonbridging oxygens in the melt, and that some, perhaps all, the Al in SA10 is a network modifier.

In composition SAN3, approximately one half of the Al^{3+} is balanced with Na^{+}. In that composition the frequencies of the two $Si–O^0$ antisymmetric stretch bands are lowered slightly relative to their frequencies in pure SiO_2, thus indicating some Si(Al) coupling. The Si/(Si + Al) of the three-dimensional network cannot be significantly less than 0.95 (compare Figs. 6 and 7).

The intensity of the band near 1100 cm^{-1} in SAN3 melt is diminished relative to the overall intensity of the high-frequency envelope compared with the data for SA10 melt. This decrease is consistent with the fact that less Al^{3+} may be a network modifier in SAN3 melt than in SA10 melt. The spectra of SA10 and SAN3 melts are quite similar, however, which leads to the conclusion that the structures of the two melts are similar.

The $NaAlSi_7O_{16}$ quenched melt is fully polymerized, as discussed under $NaAlO_2$–SiO_2 spectra above (Fig. 5).

The effect of pressure on melt structure

Binary joins. The Raman spectra of NS, NS2, NS3 and Di melts quenched from pressures up to 20 kbar are identical to the one-atm spectra within experimental uncertainty (Table 2). We conclude, therefore, that there is no discernible pressure dependence of the anionic structure of these melts.

The join $NaAlO_2$–SiO_2. Two melt compositions, $NaAlSi_3O_8$ (Ab) and $NaAlSi_2O_6$ (Jd), were subjected to up to 38 kbar pressure. The detailed Raman spectroscopic data resulting from these experiments are shown in Table 4, with deconvoluted high-frequency envelopes in Figure 8. The overall appearance of the spectra is not affected by pressure. If, for example, some Al^{3+} were to leave the network to form AlO_6 clusters or octahedra, bands due to nonbridging oxygen are expected (see Fig. 7).

The only observable spectroscopic change in samples quenched at high pressure is an increase in the intensity of the I_2 band relative to the I_1 band in the high-frequency envelope (Table 4). This change may indicate that the overall proportion of the most aluminous, three-dimensional network structure in the melt has increased relative to the less aluminous structural unit. The same trend was observed at 1 atm as the Si/(Si + Al) of melts on the join $NaAlO_2$–SiO_2 decreased. On that join, the Si/(Si + Al) of the two structural units also displayed a decrease, an effect that is not observed as the pressure is increased on a given composition (Figs. 7 and 8; see also Table 4).

Discussion

Structural models of silicate melts

The most important observation made from the above assignment of the Raman spectra is that there is a unique set of coexisting anionic structural units for specific ranges of the ratio of nonbridging oxygen to silicon. In Table 3, the anionic units are defined on the basis of average NBO/Si. There are several aspects of these conclusions that warrant further comment. In comparison to some models of melt structure (*e.g.*, Masson, 1977), the present model is strikingly simple. This simplicity should not be surprising in view of the fact that when comparing the crystal structures of silicate minerals, only a few structural arrangements can be found (see Dent Glasser, 1979, for review). In fact, in silicate crystal chemistry, the metal cations are considered very important in controlling the type of polymers that will occur. Polymer theory as applied to silicates (*e.g.*, Masson, 1977) does not take metal cations into account.

Previous models of melt structures include features such as trimers, tetramers, pentamers, *etc.*, in addition to rings and branched chains. The experimental basis for most of these models has been chromatographic data derived from trimethylsilyl derivatives of the silicate polymers (TMS derivatives). When applying that method to glass structural determinations, certain inconsistencies are found. First, when comparing the results from TMS derivatives to structural data derived from Raman spectroscopy of the same materials, the results differ (compare, for example, the results of Lentz, 1964 with Brawer and White, 1975 for the system Na_2O–SiO_2, and the data for the system PbO–SiO_2 by Smart and Glasser, 1978 and Furukawa *et al.*, 1978). Second, the results obtained with chromatographic characterization of TMS derivatives are internally inconsistent. Furthermore, the yield of the derivation technique is never 100%. For example, Lentz (1964) published results for the proportion of structural units in $2Na_2O \cdot SiO_2$ glass, which produced monomers (43.5%), dimers (19.8%), trimers (10.0%), and tetramers (9.6%). These propor-

tions total to 87.9%. The bulk NBO/Si of this total is 2.84. If it is assumed that the remainder of the material is that of a pentamer (NBO/Si = 2.4), addition of this proportion to that total NBO/Si yields bulk NBO/Si = 2.79 for $2Na_2O \cdot SiO_2$ glass. If the unreacted remainder included polymers that were more polymerized than that of a pentamer, the bulk NBO/Si would be even smaller. For lead orthosilicate (Smart and Glasser, 1978), the result of a similar calculation is NBO/Si = 2.76. Inasmuch as orthosilicates have an overall NBO/Si = 4, the results from TMS derivatives indicate that the silicate polymers condensed during preparation of the derivative. Similar results are obtained when calculating bulk NBO/Si for more silica-rich glasses. The existence of such problems has been further documented by Kuroda and Kato (1979), who showed that the chromatographic results depended on the type of silylating agent used to form the derivatives.

Another feature of polymer models for silicate melt structure is a positive correlation between order and proportion of silicate polymers and bulk NBO/Si of the melt. In Raman spectroscopic studies, such an evolution would result in a successive increase of the frequency of Si–O stretch bands as the number of Si^{4+} cations in the polymers increases (*e.g.*, Lazarev,

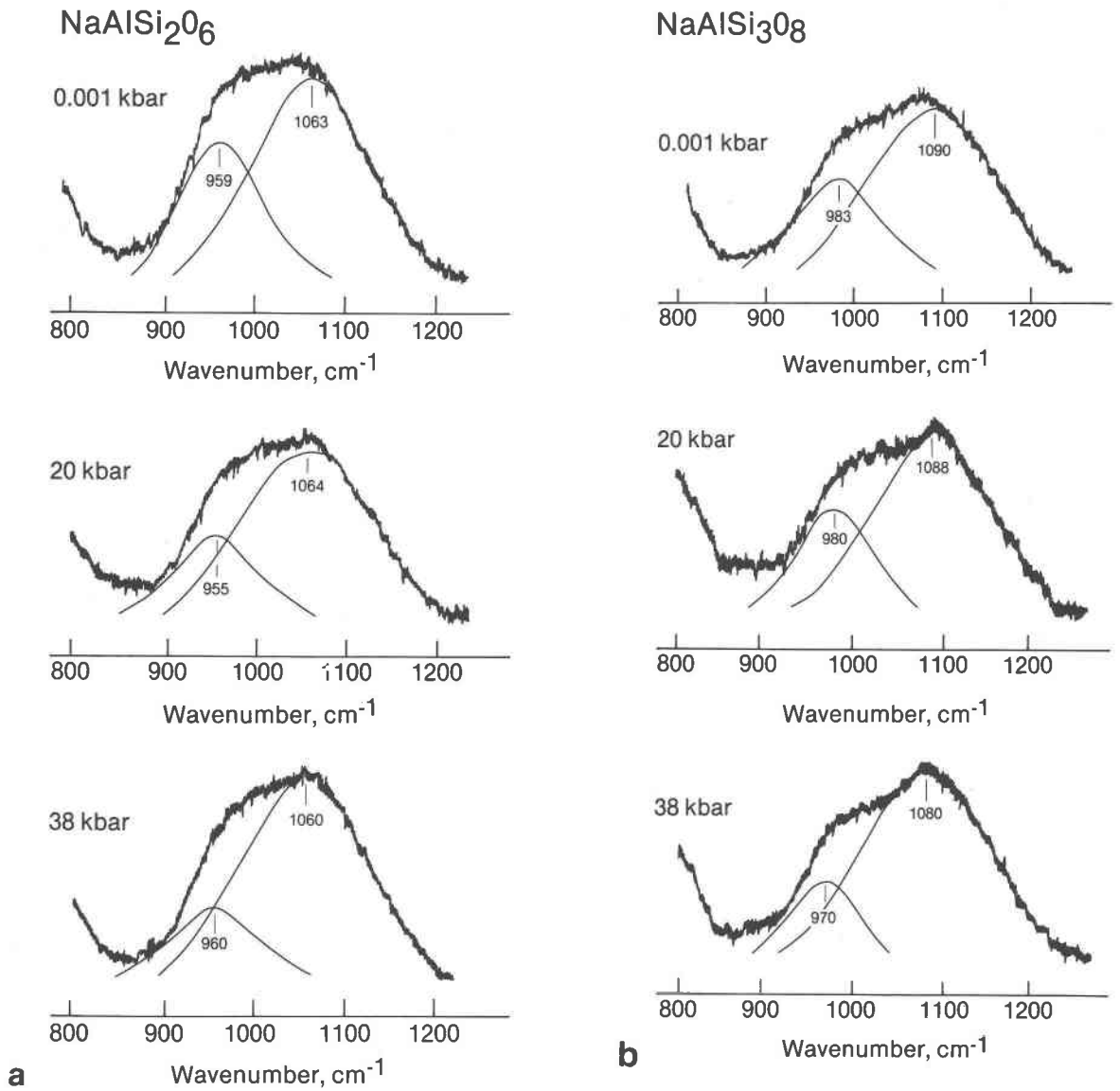

Fig. 8. Raman spectra of quenched $NaAlSi_2O_6$ (a) and $NaAlSi_3O_8$ (b) melts as a function of pressure.

1972; Brawer and White, 1975; Furukawa and White, 1980; see also Table 3). On this basis it would be expected that if anionic structural units with degree of polymerization between dimers and chains were formed in melts on the various binary silicate joins such as those discussed above (see Figs. 2 and 3), new bands would occur or bands such as that near 900 cm^{-1} would shift to higher frequency as the M/Si of the melt is decreased. There is no such spectroscopic evidence in our data or in any related published data (Brawer and White, 1975, 1977; Furukawa *et al.*, 1978; Verweij and Konijnendijk, 1976; Verweij, 1979a,b; Furukawa and White, 1980). We conclude, therefore, that structural units with NBO/Si between that of a dimer and that of a chain (3 and 2, respectively) do not exist in significant amounts in silicate melts.

The structural unit with NBO/Si = 2 has been referred to as a chain structure. Ring structures have, however, the same NBO/Si. The idea of ring structures in silicate melts has experimental support in experimental studies of TMS derivatives of silicate melts (*e.g.*, Masson, 1977). Ring structures have also been suggested in melts on binary alkali metal–silicate joins on the basis of the viscous behavior of such melts (*e.g.*, Tomlinson *et al.*, 1958; Mackenzie, 1960, p. 205; Bockris and Reddy, 1970, p. 612). In view of the discussion above, it is not clear whether TMS data give an accurate description of the structure of the melt.

Mass balance considerations require that the melts with M, C, and S-bands need at least one structural unit with NBO/Si less than 2. We suggest that the S-band in Figures 2 and 3 reflects vibrations in such a structural unit. Consider, for example, the spectrum of Wo ($CaSiO_3$) in Figure 2. The Wo composition has bulk NBO/Si = 2. The strong 870 cm^{-1} and an even stronger 970 cm^{-1} band are due to the presence of structural units in the melt with 4 and 2 NBO/Si, respectively. In order to maintain mass balance of oxygen and silicon, there must be structural units in this melt that have NBO/Si less than 2. Careful analysis by in particular Verweij (1979a,b) and Furukawa and White (1980) and also by Virgo *et al.* (1980) has led to the conclusion that the band in the frequency range between 1070 and 1100 cm^{-1} in the $MO–SiO_2$ and $M_2O–SiO_2$ melts most likely is a stretch vibration from a unit that has NBO/Si = 1. One might suggest that such a vibrational mode could stem from end units in a linear structure. Such an interpretation does not, however, provide for structural units that satisfy the mass balance of the melt. It might also be suggested that the presence of branched chains or multiple chains in the melt constitutes the structural unit(s) with NBO/Si less than 2. The end result of the evolution of such branching is, of course, an infinite sheet. The frequency of the band in question (denoted S in Figs. 2 and 3) does not shift with changes in M/Si. Its intensity increases with decreasing M/Si, however. On this basis, we conclude that the NBO/Si of this structural unit does not vary with changes of bulk NBO/Si of the melt. The possibility of a branched chain is considered unlikely for two reasons. First, there is no experimental evidence for the presence of such structures in silicate melts (branched chains with NBO/Si less than 2). Second, according to a survey by Dent Glasser (1979), branched chains do not occur in minerals. Instead, chains and sheets are formed. There is no clear reason, therefore, why one would expect such a structure in a melt.

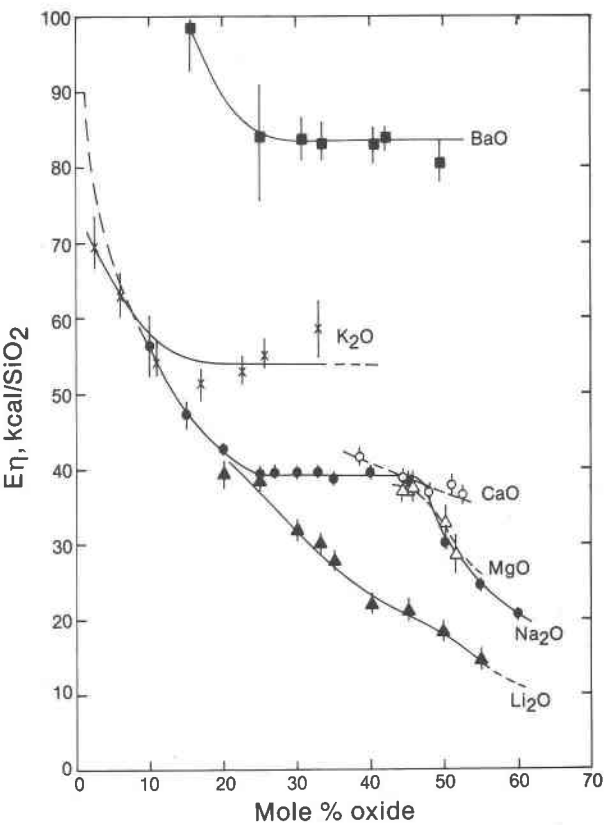

Fig. 9. Activation energy of viscous flow of binary melts on alkali metal–silicate and alkaline earth–silicate joins. The activation energy (E_η) is recalculated to a constant number of SiO_2 units (1). Data from Bockris and Löwe (1954), Bockris *et al.* (1955), MacKenzie (1960, p. 201) and summary of data by Bockris and Reddy (1970, p. 604).

An option that does exist to explain the 1070 cm^{-1} is multiple chains. It cannot be established from the Raman data whether the S-band (Figs. 2 and 3) is due to an infinite sheet or a finite sheet (*e.g.*, multiple chains). In view of the data summarized above, it is most likely that the structural unit has an average NBO/Si near 1 (infinite sheet), and the structural units represented by this Si–O stretch band in the Raman spectra will be referred to as a sheet.

Because the relative integrated intensities of the bands assigned to the different anionic species may not be linearly related to NBO/Si, only a general discussion of their relative abundances in these silicate melts is possible at this time. We suggest that monomers are the most abundant species in the melts near the orthosilicate composition and that they become increasingly unstable with decreasing NBO/Si but are still present in the $CaSi_2O_5$ sheet composition. In contrast, the dimer unit has a restricted range of stability, with an apparent maximum in its abundance between the ortho- and metasilicate compositions. The instability of the dimer species appears to coincide with the appearance of the sheet unit, and with increasing NBO/Si the sheet and chain species increase in abundance relative to the monomer units.

From the above discussion, we propose that the equilibria relating the coexisting anionic species (units) in silicate melts can be expressed with the following equations:

For $4 > \text{NBO/Si} > 2$:

$$2Si_2O_7^{6-} \rightleftarrows 2SiO_4^{4-} + Si_2O_6^{4-} \quad (1)$$

for $2 > \text{NBO/Si} > 1$:

$$3Si_2O_6^{4-} \rightleftarrows 2SiO_4^{4-} + 2Si_2O_5^{2-} \quad (2)$$

and for $1 > \text{NBO/Si} > 0.1$:

$$2Si_2O_5^{2-} \rightleftarrows Si_2O_6^{4-} + 2SiO_2 \quad (3)$$

This model of the anionic structure of silicate melts delineates three distinct compositional regions. Inside each region a combination of three anionic structural units occurs. The Raman spectra provide little information about the metal cation–oxygen polyhedra.

Melt structure and physical properties

Binary joins. Data on thermal expansivity (*e.g.*, Tomlinson *et al.*, 1958; Bockris and Kojonen, 1960; Robinson, 1969) indicate no compositional dependence of this parameter in the compositional regions with less than about 10–15 mole % metal oxide. Those authors concluded, therefore, that the melts are essentially made up of three-dimensional SiO_2 units where Na^+ cations, for example, are trapped in "holes" in the melt. Thermal expansivity increases rapidly as the molar metal oxide content is increased beyond about 10%, which leads to the conclusion that nondirectional anionic, metal–oxygen bonds are responsible for the melt expansivity (Tomlinson *et al.*, 1958). Bockris and Reddy (1970, p. 615) pointed out, however, that partial molar volume data for SiO_2 in the same melts indicate that discrete SiO_2 "icebergs" must remain in the structure to at least 33 mole % metal oxide. These observations are consistent with the Raman spectroscopic data. The data (Fig. 1) were interpreted to indicate that binary metal oxide–silicate melts break down into at least three structural units at about 10 mole % metal oxide. These structural units are of three-dimensional type, of sheet type (NBO/Si = 1), and of chain type (NBO/Si = 2). We conclude, therefore, that the interpretation of the Raman data leads to a structural model that accords with thermal expansivity and partial molar volume data.

The viscosity data of silicate melts on binary metal oxide–silicate joins (*e.g.*, Bockris *et al.*, 1955; Bockris and Löwe, 1954; Tomlinson *et al.*, 1958; MacKenzie, 1960, p. 201) are particularly relevant to the anionic structure of the melts. Bockris and Reddy (1970, p. 604), in a summary of these data, concluded that the activation energy of viscous flow, $E\eta$, show three distinct regions. The $E\eta$ decreases rapidly as metal oxide is added to SiO_2 until about 20 mole % oxide is dissolved in the melt, followed by a plateau that extends to about 50 mole % metal oxide. A further increase in the metal content results in the activation energy falling. To a first approximation, the contributions to $E\eta$ are from breakage of Si–O bridging bonds and perhaps from M–O bonds so as to form an entity in the melt that can move from one location to another in the melt (flow unit) during viscous flow. In fact, Bockris and Reddy (1970, p. 600) concluded that the value of $E\eta$ was primarily a function of the heat of dissociation of Si–O bridging oxygen bonds (~104 kcal/mole). A second contribution may derive from the energy required to form the new volume ("hole") into which the flow unit moves (Glasstone *et al.*, 1941, p. 481). The latter contribution may be more important for an understanding of the absolute melt viscosity values (Lacy, 1968) than for the activation energy of viscous flow (Bockris and Reddy, 1970, p. 600). In fact, Bockris and Reddy (1970, p. 600) concluded that the value of $E\eta$ was primarily a function of the heat of dissociation of Si–O bridging oxygen bonds (~104 kcal/mole).

If it is assumed that the energy of dissociation of Si–O bonds does not vary significantly with type of metal cation, the arguments by Bockris and Reddy (1970, p. 600) and MacKenzie (1960, p. 201) may be used to calculate the average number of nonbridging oxygens per silicon that must be broken to generate the flow unit. This value may then be added to the original NBO/Si of the melt to calculate the average number of nonbridging oxygen per silicon in the flow unit [(NBO/Si)η]. In order to carry out this calculation, the Eη must be converted from kcal/mole(gram-formula weight) to kcal/Si or kcal/SiO_2. The results of such calculations are shown in Figure 9. The data base for Figure 9 is limited in that only a few oxides have been studied over the compositional range of the suggested three compositional regions delineated by Bockris and Reddy (1970, p. 604). Note that in the systems that cover the compositional range from pure SiO_2 to >50 mole % metal oxide, the Eη curves define three compositional regions similar to those summarized by Bockris and Reddy. These compositional regions correspond to the regions of structural similarity described in equations 1–3, within experimental uncertainty.

It appears from the data in Figure 9 that for a given mole % metal oxide components, the Eη (in kcal/SiO_2) increases with increasing metal cation size. For metal cations of a fixed size, the activation energy of viscous flow increases as the valence of the cation increases. If in fact the dissociation energy of the bridging Si–O bonds is not affected significantly by the type of metal cation, and there is no significant contribution from M–O bonds to the value of the activation energy, the data in Figure 9 imply that the average NBO/Si of the flow units during viscous flow depends on the type of cation (Fig. 10). The average (NBO/Si)η shown in Figure 10 is derived on the basis that the energy of dissociation of the bridging oxygen bonds is the only contribution to the value of Eη. Metal–oxygen bonds and steric considerations are not included. We conclude, therefore, that the values of (NBO/Si)η in Figure 10 are minimum values.

Another consequence of the above observations is that the constancy of Eη over a given range of M/Si requires that the average size of the flow unit decreases with increasing M/Si (Fig. 10). This conclusion differs from that of Bockris and coworkers and MacKenzie and coworkers (Bockris *et al.*, 1955, 1956; MacKenzie, 1960, p. 205; Bockris and Reddy, 1970, p. 614). Those authors proposed a "polyanionic structure" model where in a given compositional

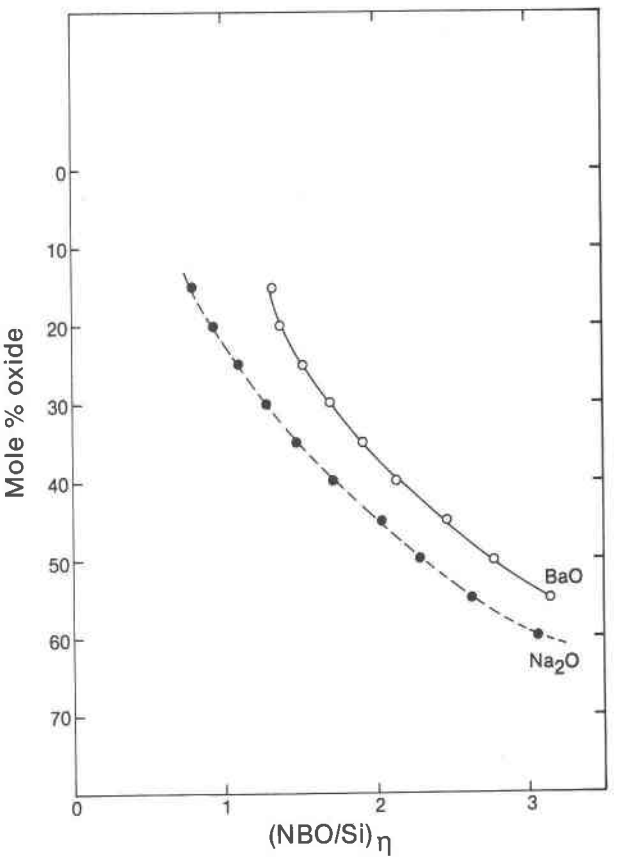

Fig. 10. Calculated minimum number of nonbridging oxygens per silicon in flow units on the joins Na_2O–SiO_2 and BaO–SiO_2. See text for further explanation.

range the consequence of constant Eη is that the types of structural units in the melt and the types of flow units must be the same. Our conclusions are that the types of structural units in the melt are similar over the individual compositional ranges, but the size of the flow unit may vary. The data in Figure 10 indicate that the average size of the flow unit decreases with increasing M/Si, an observation that accords with the observation that the absolute viscosity of the melts decreases as the M/Si decreases (see Bottinga and Weill, 1972, for summary of data).

Aluminosilicate melts with charge-balanced Al^{3+}. Viscosity, thermal expansion, and thermochemical data (Riebling, 1966; Navrotsky *et al.*, 1980) have been used to suggest that melt compositions along the join $NaAlO_2$–SiO_2 are structurally similar. Structural data by Taylor and Brown (1979) agree with the present data in that these melts have a three-dimensional network structure. The Raman data shown here also indicate, however, that there may be two anionic three-dimensional structural units in the

melts. These two units differ in their Si/(Si + Al), whereas the value of this ratio in both units decreases with decreasing bulk Si/(Si + Al).

The activation energy of viscous flow in SiO_2 melt is about twice that of $NaAlSi_3O_8$ melt (Riebling, 1966). Inasmuch as these two melts appear to have the same structural features, it has frequently been suggested that the decrease of η and $E\eta$ with increasing Al content is due to the increased proportion of weaker Al–O relative to Si–O bonds (*e.g.*, Taylor and Rindone, 1970). The energy of dissociation of the bridging Al–O bonds is likely to depend on the type of metal cation needed for local charge balance of Al^{3+} in tetrahedral coordination. Both η and $E\eta$ are lowered with decreasing radius of the charge-balancing cation and with increasing electrical charge (Rossin *et al.*, 1964; Hofmaier, 1968; Riebling, 1964, 1966; see also Bottinga and Weill, 1972 and Cukierman and Uhlmann, 1973). For example, the viscosity of $NaAlSiO_4$ melt is nearly an order of magnitude greater than that of $CaAl_2Si_2O_8$ melt ($X^{mole}SiO_2 = 0.5$ in both melts). The viscosity of $MgAlO_2$–SiO_2 and $BaAlO_2$–SiO_2 melts at $X^{mole}SiO_2 = 0.75$ is near 10^3 poise for the former and $\sim 10^5$ poise for the latter melt. We suggest, therefore, that the strength of the Al–O bridging bonds (heat of dissociation) in three-dimensional aluminosilicate melts decreases as the size of the charge-balancing cation decreases and as its electrical charge increases. The absolute values of the energy of dissociation of these bonds as a function of such variables is not known. It is not possible, therefore, to estimate the size of the flow units on this basis. The Raman data may be used to suggest a model for at least some aspects of viscous flow in $NaAlO_2$–SiO_2 melt and probably also other $MAlO_2$–SiO_2 and MAl_2O_4–SiO_2 melts. On the basis of the Raman data we suggest that the most Si-rich three-dimensional structural units may represent the actual flow units, whereas the majority of the Al–O bonds that will be broken to form the flow unit is derived from the most Al-rich structural unit in the melt.

Aluminosilicate melts with $Na/Al < 1$. The viscosity and activation energy of viscous flow decreases rapidly as Al^{3+} is added to melts on the join $NaAlO_2$–SiO_2 (Riebling, 1966). Lacy (1968) commented that there is a positive correlation between NBO/Si of a melt and its viscosity. This conclusion accords with the Raman data, which indicate that nonbridging oxygens are formed as Na^+/Al^{3+} of the melts is lowered below 1 (Fig. 7).

Effect of pressure. The pressure dependence of the viscosity of four melt compositions in the binary joins discussed above was determined by Kushiro (1976) and Scarfe *et al.* (1979). Of these melts, those of Di, NS, and NS2 composition have $(d\eta/dP)_T$ positive, whereas NS3 quenched melt has negative pressure dependence of the viscosity (Table 5). Unfortunately, no data are available on the activation energy of viscous flow of these melts. It is difficult, therefore, to assess whether the flow mechanisms of these melts change with pressure. There is no significant change of the anionic structure of these melts with increasing pressure, although the proportion of the least polymerized unit (monomer) seems to decrease with increasing pressure. Intuitively, such an evolution may result in increased steric hindrance of viscous flow.

Scarfe *et al.* (1979) noted that the compressibility of melts with a negative pressure dependence of vis-

Table 5. Changes (percentage relative to values at 1 atm) of physical properties between 1 atm and high pressure

Composition (pressure and temperature)	NBO/T	Viscosity	Density	Reference
$CaMgSi_2O_6$ (0.001-15 kbar, 1640°C)	2	+267	+8.3	Scarfe et al. (1979)
Na_2SiO_3 (0.001-20 kbar, 1300°C)	2	+650	+6.7	Scarfe et al. (1979)
$Na_2Si_2O_5$ (0.001-15 kbar, 1200°C)	1	+311	+6.3	Scarfe et al. (1979)
$K_2O{\cdot}MgO{\cdot}5SiO_2$ (5-20 kbar, 1300°C)	0.8	-64	...	Kushiro (1977)
$Na_2Si_3O_7$ (0.001-20 kbar, 1175°C)	0.67	-65	...	Kushiro (1976)
$NaAlSi_2O_6$ (0.001-20 kbar, 1350°C)	0	-90	...	Kushiro (1976)
$NaAlSi_2O_8$ (0.001-20 kbar, 1400°C)	0	-84	+21.2	Kushiro (1978a)
Olivine tholeiite (Kilauea, 1921) (0.001-20 kbar, 1400°C)	0.76	-51	+12.2	Fujii and Kushiro (1977)
Abyssal tholeiite (45-395A-8-1-9) (0.001-12 kbar, 1300°C)	0.66	-57	+7.1	Fujii and Kushiro (1977)
Crater Lake andesite (0.001-20 kbar, 1350°C)	0.27	-51	...	Kushiro et al. (1976)

cous flow is much greater than those of melts with a positive pressure dependence (see also Table 5). The Raman spectra, however, demonstrate that the melts do not show significant changes of their anionic structure as a function of pressure (Table 2). In contrast to the observation at 1 atm, where the decrease of η and $E\eta$ may be related to increasing $NaAlO_2/SiO_2$, there is no spectroscopic evidence for any change of Si/(Si + Al) of the structural units as a function of pressure. The thermal expansivity of these melts is negligible (Riebling, 1964, 1966). Bockris *et al.* (1956) and Bockris and Reddy (1970, p. 615) suggested that thermal expansion was primarily due to expansion of M–O polyhedra, and that such expansion could only take place when the melt consisted predominantly of large, discrete polyanions. Evidently this reasoning does not apply to compression of melts, because the largest compressibility is found in melts with the smallest thermal expansivity.

An explanation of the large compressibility may be a collapse of the three-dimensional network structure around the metal cation. This collapse may result in an increased number of nearest oxygen neighbors of the metal cation. Consequently, Brown (1978) suggested that the effective valence of each oxygen may decrease. A consequence of such an effect would be a decrease of the strength of the Al–O bonds, as the effect would be the same as a decrease in the size of the metal cation at 1 atm. The result of this collapse is, therefore, a decreased viscosity and activation energy of viscous flow of the melts along the join $NaAlO_2$–SiO_2 as a function of pressure. It is also likely that other aluminosilicate melts would show a decrease in η and $E\eta$ with increasing pressure.

Applications

Melt structures can be described in terms of three-dimensional network units, sheets, chains, dimers, and monomers. When the proportions of structural units in natural magma are calculated, Al^{3+}, Ti^{4+}, and P^{5+} must be considered part of the network structure. Ferric iron is a network former only when sufficient alkalies are present for local charge balance (Mysen *et al.*, 1980a; Seifert *et al.*, 1979b). The result of calculations of the proportions of structural units in natural magma where their pressure dependence of viscosity is known (Table 5) is shown in Table 6. In these calculations, it was assumed that alkali aluminates ($MAlO_2$) were formed in preference to other complexes such as $MFeO_2$. Any M cation left over after the formation of $MAlO_2$ would form $MFeO_2$. Any alkali excess over that needed to form $MFeO_2$ is considered a network modifier. Any Fe^{3+} left over after all the alkali metals have been consumed is also considered a network modifier. If there is insufficient alkali metal present to transform the aluminum to $MAlO_2$, the alkaline earths are used to form MAl_2O_4 complexes. The proportions of tetrahedral cations thus calculated are assigned to structural units in the melt. Table 6 shows that basalt has NBO/T near that of $Na_2Si_3O_7$ composition. The andesite melt is even more polymerized. In view of the mechanisms for viscous flow discussed above, the observed negative pressure dependence of their viscosity is expected.

Table 6. Compositions of rocks for which the pressure dependence of their viscosity is known

	1	2	3
SiO_2	49.16	50.0	59.46
TiO_2	2.29	1.64	0.73
Al_2O_3	13.33	15.0	17.90
Fe_2O_3	1.31	--	--
FeO	9.71	11.2*	5.18*
MnO	0.16	0.22	0.10
MgO	10.41	8.40	3.71
CaO	10.93	10.60	6.45
Na_2O	2.15	2.70	4.23
K_2O	0.51	0.13	1.47
P_2O_5	0.16	--	--
NBO/T	0.76	0.66	0.27

1. Kilauea 1921 olivine tholeiite (Yoder and Tilley, 1962).
2. Abyssal tholeiite 45-395-8-1-9 (Fujii and Kushiro, 1977).
3. Crater Lake andesite (Kushiro et al., 1976).

* All iron as FeO.

For melts with constant NBO/T, the values of viscosity and activation energy of viscous flow depend on the proportion and strength of T–O^0 bonds (where T cations do not include Si^{4+}). For example, we suggest that the melt viscosity will decrease with increasing Na^+/K^+, Ca^{2+}/Mg^{2+}, and Ca^{2+}/Na^+ of the melt. It is also likely that with Fe^{3+} as a network former, the viscosity of the melt will decrease with increasing Fe^{3+}/Al^{3+}. The latter effect may be observed if the redox ratio (Fe^{3+}/Fe^{2+}) of a peralkaline magma [$(Fe^{3+} + Al^{3+}) < (Na^+ + K^+)$] were allowed to increase.

It has been observed that the viscosity of hydrous andesite and granite melt tends to increase with increasing pressure, even though their anhydrous equivalents show a negative pressure dependence of viscosity (Shaw, 1963; Kushiro, 1978c; Kushiro *et al.*, 1976). Inasmuch as solution of H_2O in such melts results in a significant increase of NBO/T (Mysen *et al.*, 1980b), it is likely that the mechanisms of viscous

flow of such melts resemble that of binary metal oxide–silicate melt, where, in fact, the viscosity increases with increasing pressure.

Basanites and picrites have NBO/T between 1 and 2. We suggest, therefore, that magmas of such compositions will show a viscosity increase with increasing pressure. The pressure effect is likely to be greater for picrite than for basanite melt because the NBO/T is greater in picrite than in basanite.

Acknowledgments

Critical reviews by I. Kushiro, E. Takahashi, and H. S. Yoder, Jr. are appreciated. Reviews by G. E. Brown, G. Waychunas, S. A. Brawer, and H. S. Waff of an early version of this manuscript greatly improved the paper.

Scarfe acknowledges support from the Carnegie Institution of Washington and Canadian NSERC grant A 8394.

This research was partially supported by NSF grant EAR 7911313 and partially by the Carnegie Institution of Washington.

References

Arndt, N. T. (1977) Ultrabasic magmas and high-degree melting of the mantle. *Contrib. Mineral. Petrol., 64,* 205–221.

Bando, Y. and K. Ishizuka (1979) Study of the structure of silica glass by high-resolution electron microscopy. *J. Non-Cryst. Solids, 33,* 375–382.

Bartlett, R. W. (1969) Magma convection, temperature distribution and differentiation. *Am. J. Sci., 267,* 1067–1082.

Bates, J. B., R. W. Hendricks and L. B. Shaffer (1974) Neutron irradiation effects and the structure of noncrystalline SiO_2. *J. Chem. Phys., 61,* 4163–4176.

Bell, R. J. and P. Dean (1970) Atomic vibrations in vitreous silica. *Disc. Faraday Soc., 50,* 55–61.

——— and ——— (1972) Localization on phonons in vitreous silica and related glasses. In R. W. Douglas and B. Ellis, Eds. *International Conf. on the Physics of Non-Crystalline Solids,* 3rd ed., p. 443–452. Wiley-Interscience, London.

Bockris, J. O'M. and F. Kojonen (1960) The compressibility of certain molten alkali silicates and borates. *J. Am. Ceram. Soc., 82,* 4493–4497.

——— and D. C. Löwe (1954) Viscosity and the structure of molten silicates. *Trans. Faraday Soc., 51,* 1734–1748.

——— and A. K. N. Reddy (1970) *Modern Electrochemistry,* vol. 1. Plenum Press, New York.

———, J. D. MacKenzie and J. A. Kitchner (1955) Viscous flow in silica and binary silicates. *Trans. Faraday Soc., 51,* 1734–1748.

———, J. W. Tomlinson and J. L. White (1956) The structure of liquid silicates. *Trans. Faraday Soc.. 52,* 299–311.

Bottinga, Y. and D. F. Weill (1972) The viscosity of magmatic silicate liquids: a model for calculation. *Am. J. Sci., 272,* 438–475.

Boyd, F. R. and J. L. England (1960) Apparatus for phase equilibrium measurements at pressures up to 50 kilobars and temperatures up to 1750°C. *J. Geophys. Res., 65,* 741–748.

Brawer, S. A. (1975) Theory of the vibrational spectra of some network and molecular glasses. *Phys. Rev., B11,* 3173–3194.

——— and W. B. White (1975) Raman spectroscopic investigation of the structure of silicate glasses. I. The binary silicate glasses. *J. Chem. Phys., 63,* 2421–2432.

——— and ——— (1977) Raman spectroscopic investigation of the structure of silicate glasses. II. Soda-alkali earth alumina ternary and quaternary glasses. *J. Non-Cryst. Solids, 23,* 261–278.

Brown, I. D. (1978) Bond valences—a simple structural model for inorganic chemistry. *Chem. Soc. (London) Rev., 7,* 359–376.

Cukierman, M. and D. R. Uhlmann (1973) Viscosity of liquid anorthite. *J. Geophys. Res., 78,* 4920–4924.

Day, D. E. and G. E. Rindone (1962a) Properties of soda aluminosilicate glasses. III. Coordination of aluminum ions. *J. Am. Ceram. Soc., 45,* 579–587.

——— and ——— (1962b) Properties of aluminosilicate glasses. II. Internal friction. *J. Am. Ceram. Soc., 45,* 496–504.

Dent Glasser, L. S. (1979) Non-existent silicates. *Z. Kristallogr., 149,* 291–305.

Eggler, D. H. (1977) Calibration of a Pyrex solid-media assembly. *Carnegie Inst. Wash. Year Book, 76,* 656–658.

Etchepare, J. (1972) Study by Raman spectroscopy of crystalline and glassy diopside. In R. W. Douglas and B. Ellis, Eds., *Amorphous Materials,* p. 337–346. Wiley, New York.

Flood, H. and W. J. Knapp (1968) Structural characteristics of liquid mixtures of feldspar and silica. *J. Am. Ceram. Soc., 51,* 259–263.

Fujii, T. and I. Kushiro (1977) Melting relations and viscosity of an abyssal tholeiite. *Carnegie Inst. Wash. Year Book, 76,* 461–465.

Furukawa, T. and W. B. White (1980) Raman spectroscopic investigation of the structure of silicate glasses. III. Alkali-silico-germanates. *J. Chem. Phys.,* in press.

———, S. A. Brawer and W. B. White (1978) The structure of lead silicate glasses determined by vibrational spectroscopy. *J. Mat. Sci., 13,* 268–282.

Galeener, F. L. and G. Lucovsky (1976a) Longitudinal optical vibrations in vitreous SiO_2. In G. Lucovsky and F. L. Galeener, Eds., *Int. Conf. on Structure and Oscillations of Amorphous Solids.* Am. Inst. Physics.

——— and ——— (1976b) Longitudinal optical vibrations in glasses: GeO_2 and SiO_2. *Phys. Rev. Lett., 37,* 1474–1478.

Gaskell, P. M. (1975) Construction of a model for amorphous tetrahedral materials using ordered units. *Phil. Mag., 32,* 211–229.

——— and A. B. Mistry (1979) High-resolution transmission electron microscopy of small amorphous silica particles. *Phil. Mag., 39,* 245–257.

Glasstone, S., K. Laidler and H. Eyring (1941) *The Theory of Rate Processes.* McGraw-Hill, New York.

Hofmaier, G. (1968) Viskosität und Struktur flüssiger Silikate. *Berg Huettenmaenn. Monatsh. Montan. Hochsch. Loeben, 113,* 270–281.

Kracek, F. C. (1930) The system sodium oxide–silica. *J. Phys. Chem., 34,* 1583–1598.

Kuroda, K. and C. Kato (1979) Trimethylsilylation of hemimorphite. *J. Inorg. Nucl. Chem., 41,* 947–951.

Kushiro, I. (1976) Changes in viscosity and structure of melts of $NaAlSi_2O_6$ composition at high pressures. *J. Geophys. Res., 81,* 6347–6350.

——— (1977) Phase transformation in silicate melts under upper mantle conditions. In M. H. Manghnani and S. Akimoto, Eds., *High-Pressure Research: Applications in Geophysics,* p. 25–37. Academic Press, New York.

——— (1978a) Viscosity and structural changes of albite ($NaAlSi_3O_8$) melt at high pressure. *Earth Planet. Sci. Lett., 41,* 87–91.

——— (1978b) Viscosity changes of GeO_2 melt as a model of SiO_2 melt with high pressure. *Carnegie Inst. Wash. Year Book, 77,* 672–675.

——— (1978c) Density and viscosity of hydrous calc-alkalic magma at high pressure. *Carnegie Inst. Wash. Year Book, 77,* 675–677.

———, H. S. Yoder, Jr. and B. O. Mysen (1976) Viscosities of basalt and andesite melts at high pressures. *J. Geophys. Res., 81,* 6351–6356.

Lacy, E. D. (1963) Aluminum in glasses and melts. *Phys. Chem. Glasses, 4,* 234–238.

——— (1968) Structure transition in alkali silicate glasses. *J. Am. Ceram. Soc., 51,* 150–157.

Lazarev, A. N. (1972) *Vibrational spectra and structure of silicates.* Consultants Bureau, New York.

Lentz, C. W. (1964) Silicate minerals as sources of trimethylsilyl silicates and silicate structure analysis of sodium silicate solutions. *Inorg. Chem., 3,* 574–579.

Lucovsky, G. (1979a) Defect-controlled carrier transport in amorphous SiO_2. *Phil. Mag., 39,* 531–541.

——— (1979b) Spectroscopic evidence for valence-alternation defects in vitreous SiO_2. *Phil. Mag., 39,* 513–531.

MacKenzie, J. D. (1960) Structure of some inorganic glasses from high temperature studies. In J. D. MacKenzie, Ed., *Modern Aspects of the Vitreous State,* p. 188–218. Butterworth's, Washington, D. C.

Mao, H. K., P. M. Bell and J. L. England (1971) Tensional errors and drift of thermocouple electromotive force in the single-stage, piston–cylinder aparatus. *Carnegie Inst. Wash. Year Book, 70,* 281–287.

Marsh, B. D. (1975) Plume spacing and the source. *Nature, 256,* 240.

Masson, C. R. (1977) Anionic constitution of glass-forming melts. *J. Non-Cryst. Solids, 1,* 1–42.

Mysen, B. O., F. Seifert and D. Virgo (1980a) Structure and redox equilibria of iron-bearing silicate melts. *Am. Mineral.,* in press.

———, D. Virgo and C. M. Scarfe (1979) Viscosity of silicate melts as a function of pressure: structural interpretation. *Carnegie Inst. Wash. Year Book, 78,* 551–556.

———, ———, W. J. Harrison and C. M. Scarfe (1980b) Solubility mechanisms of H_2O in silicate melts at high pressures and temperatures: a Raman spectroscopic study. *Am. Mineral.,* in press.

Navrotsky, A., R. Hon, D. F. Weill and D. J. Henry (1980) Thermochemistry of glasses and liquids in the systems $CaMgSi_2O_6$–$CaAl_2SiO_6$–$NaAlSi_3O_8$, SiO_2–$CaAl_2Si_2O_8$–$NaAlSi_3O_8$ and SiO_2–Al_2O_3–CaO–Na_2O. *Geochim. Cosmochim. Acta,* in press.

Riebling, E. F. (1964) Structure of magnesium aluminosilicate liquids at 1700°C. *Can. J. Chem., 42,* 2811–2821.

——— (1966) Structure of sodium aluminosilicate melts containing at least 50 mole % silica at 1500°C. *J. Chem. Phys., 44,* 2857–2865.

——— (1968) Structural similarities between a glass and its melt. *J. Am. Ceram. Soc., 51,* 143–149.

Robinson, H. A. (1969) Physical properties of alkali silicate glasses: I, additive relations in alkali binary glasses. *J. Am. Ceram. Soc., 52,* 392–399.

Rossin, R., J. Bersan and G. Urbain (1964) Étude de la viscosité de laitiers liquide appartenant au système ternaire SiO_2–Al_2O_3–CaO. *Rev. Hautes Temp. et Refractains, 1,* 159–170.

Scarfe, C. M., B. O. Mysen and D. Virgo (1979) Changes in viscosity and density of melts of sodium disilicate, sodium metasilicate and diopside composition with pressure. *Carnegie Inst. Wash. Year Book, 78,* 547–551.

Seifert, F., D. Virgo and B. O. Mysen (1979a) Sodium loss from sodium metasilicate melts in CO_2 and CO atmospheres. *Carnegie Inst. Wash. Year Book, 78,* 679.

———, ——— and ——— (1979b) Melt structures and redox equilibria in the system Na_2O–FeO–Fe_2O_3–SiO_2. *Carnegie Inst. Wash. Year Book, 78,* 511–519.

Sharma, S. K. and H. S. Yoder (1979) Structural study of glasses of akermanite, diopside and sodium melilite compositions by Raman spectroscopy. *Carnegie Inst. Wash. Year Book, 78,* 526–532.

———, D. Virgo and B. O. Mysen (1978) Structure of glasses and melts of $Na_2O \cdot xSiO_2$ (x = 1, 2, 3) composition from Raman spectroscopy. *Carnegie Inst. Wash. Year Book, 77,* 649–652.

———, ——— and ——— (1979) Raman study of the coordination of aluminum in jadeite melts as a function of pressure. *Am. Mineral., 64,* 779–787.

Shaw, H. R. (1963) Obsidian–H_2O viscosities at 1000 and 2000 bars in the temperature range 700° to 900°C. *J. Geophys. Res., 68,* 6337–6343.

——— (1965) Comments on viscosity, crystal settling and convection in granitic magmas. *Am. J. Sci., 263,* 120–152.

Smart, R. M. and F. P. Glasser (1978) Silicate anion constitution of lead silicate glasses and crystals. *Phys. Chem. Glasses, 19,* 95–102.

Stolen, R. H. and G. E. Walrafen (1976) Water and its relation to broken bonds in defects in fused silica. *J. Chem. Phys., 64,* 2623–2631.

Sweet, J. R. and W. B. White (1969) Study of sodium silicate glasses and liquids by infrared spectroscopy. *Phys. Chem. Glasses, 10,* 246–251.

Taylor, M. and G. E. Brown (1979) Structure of mineral glasses. I. The feldspar glasses $NaAlSi_3O_8$, $KAlSi_3O_8$, $CaAl_2Si_2O_8$. *Geochim. Cosmochim. Acta, 43,* 61–77.

———, ——— and P. H. Fenn (1980) Structure of silicate mineral glasses. III. $NaAlSi_3O_8$ supercooled liquid at 805°C and the effects of thermal history. *Geochim. Cosmochim. Acta, 44,* 109–119.

Taylor, T. D. and G. E. Rindone (1970) Properties of soda aluminosilicate glasses. V. Low-temperature viscosities. *J. Am. Ceram. Soc., 53,* 692–695.

Tomlinson, J. W., M. S. R. Heynes and J. O'M. Bockris (1958) The structure of liquid silicates. Part 2. Molar volume and expansivities. *Trans. Faraday Soc., 54,* 1822–1834.

Verweij, H. (1979a) Raman study of the structure of alkali germanosilicate glasses. I. Sodium and potassium metagermanosilicate glasses. *J. Non-Cryst. Solids, 33,* 41–53.

——— (1979b) Raman study of the structure of alkali germanosilicate glasses. II. Lithium, sodium and potassium degermanosilicate glasses. *J. Non-Cryst. Solids, 33,* 55–69.

——— and W. L. Konijnendijk (1976) Structural units in K_2O–PbO–SiO_2 glasses by Raman spectroscopy. *J. Am. Ceram. Soc., 59,* 517–521.

Virgo, D., B. O. Mysen and I. Kushiro (1980) Anionic constitution of silicate melts quenched at 1 atm from Raman spectroscopy: implications for the structure of igneous melts. *Science, 208,* 1371–1373.

———, F. Seifert and B. O. Mysen (1979) Three-dimensional network structures in the systems $CaAl_2O_4$–SiO_2, $NaAlO_2$–SiO_2,

$NaFeO_2$–SiO_2 and $NaGaO_2$–SiO_2. *Carnegie Inst. Wash. Year Book, 78,* 506–511.

White, W. B., T. Furukawa, I. S. T. Tsong, C. Goett, J. S. Herman, G. Hauser and C. Nelson (1979) Structure of glasses containing transition metal ions. *U.S. Dept. Energy Report, Febr. 1979.*

Yoder, H. S., Jr. and C. E. Tilley (1962) Origin of basaltic magmas: an experimental study of natural and synthetic rock systems. *J. Petrol., 3,* 342–532.

Manuscript received, September 21, 1979;
accepted for publication, March 21, 1980.